약학박사학위논문

Anticancer Activities of Psammaplin A and Halichondramide Derived from Marine Natural Products

해양 천연물 유래 사마필린 A와 할리콘드라마이드의 항암활성 연구

2016년 8월

서울대학교 대학원
약학과 천연물과학전공
신 윤 호

Anticancer Activities of Psammaplin A and Halichondramide Derived from Marine Natural Products

해양 천연물 유래 사마필린 A와
할리콘드라마이드의 항암활성 연구

지도교수 이 상 국

이 논문을 약학박사학위논문으로 제출함

2016년 6월

서울대학교 대학원
약학과 천연물과학전공
신 윤 호

신윤호의 박사학위논문을 인준함

2016년 6월

위 원 장 박 성 혁 (인)

부위원장 박 형 근 (인)

위 원 신 종 헌 (인)

위 원 박 광 균 (인)

위 원 이 상 국 (인)

Abstract

Anticancer Activities of Psammaplin A and Halichondramide Derived from Marine Natural Products

Yoonho Shin

Natural Products Science Major

College of Pharmacy

The Graduate School

Seoul National University

Natural products, derived from diverse organisms, are important sources for bioactive molecules, which have been developed to treat various human health-related symptoms. In this study, bioactive compounds with anticancer activities derived from marine natural products were identified.

Psammaplin A (PsA), a unique symmetrical bromotyrosine derived from a number of marine sponges of the order Verongida, has various bioactivities such as antimicrobial activity, cytotoxicity against the leukemia cell line, and inhibition of DNA gyrase and DNA topoisomerase. PsA is also known to be a potent inhibitor of both DNA methyltransferase (DNMT) and histone deacetylase (HDAC). In this study, the antitumor activity of PsA in human non-small cell lung cancer cell line, A549, was evaluated. Analyses showed that PsA down-regulated the protein

expression of integrin-linked kinase (ILK), a hub molecule in the phosphoinositide 3-kinase (PI3K)/AKT signaling pathway, and up-regulated phospho-LATS1 and phospho-YAP, which play key roles in the activation of the Hippo signaling pathway. Moreover, PsA decreased colony formation, migration, and invasion characteristics of A549 cells. The expression of miR-4485, a small none-coding RNA, significantly increased in PsA-treated A549 cells. Agonists and antagonists of miR-4485 modulated the cellular signaling pathway and the characteristics of A549 cells accordingly.

Further, twenty-eight synthetic analogs of PsA were examined by cell proliferation assay. A structure-activity relationship (SAR) study for measuring cytotoxicity revealed that the presence of free oxime and disulfide functional groups was responsible for high cytotoxicity. Furthermore, the bromotyrosine component in PsA was relatively tolerable and hydrophobic aromatic groups preserved the cytotoxicity. The cytotoxicity of the aromatic groups was dependent on their size and spatial geometry. Among them, a β-naphthyl derivative of PsA showed cytotoxicity comparable to that of PsA and exhibited potential *in vivo* antitumor activity.

Halichondramide (HCA), a trisoxazole-containing macrolide isolated from the marine sponge *Chondrosia corticata,* exhibits cytotoxicity and antifungal activity. In the present study, the antimetastatic activity of HCA in the highly metastatic PC3 human prostate cancer cells was measured. HCA showed potent growth inhibitory activity of the PC3 cells with an IC_{50} value of 0.81 μM. Further analysis revealed that HCA suppressed the expression of potential metastatic biomarkers,

including phosphatase of regenerating liver-3 (PRL-3), PI3K subunits, and matrix metalloproteases (MMPs) (through downregulation). HCA also modulated cadherin switching in PC3 cells.

Based on these findings, PsA, which inactivates the Hippo signaling pathway and modulates phospho-YAP expression, and HCA, which regulates cancer metastatic biomarkers and MMPs, can be regarded as potential antitumor lead compounds and might be prioritized in the development of cancer chemotherapeutic agents.

Keywords: marine natural product, psammaplin A, halichondramide, anticancer activity, hippo signaling, miR-4485, PRL-3, antimetastatic activity

Student number: 2011-21732

Table of Contents

Abstract i

Table of Contents iv

List of Figures viii

List of Tables x

Part 1: General Introduction 1

A. Background 2

1. Lung cancer 2
2. Hippo signaling pathway 3
3. microRNA 8
4. Cancer metastasis and epithelial-mesenchymal transition 10

B. The Purpose of This Study 12

Part II: Antitumor Activities of Psammaplin A and its Analogues in A549 Human Lung Cancer Cells 14

A. Introduction 15

B. Materials and Methods 17

1. Materials 17

1. 1. Reagents and antibodies 17

1. 2. Compounds 18

1. 3. Cell culture 18

2. Methods 20
2. 1. Cell proliferation assay 20
2. 2. Western blot 20
2. 3. Detection of apoptosis 21
2. 4. Measuring cell proliferation 21
2. 5. Signal Transduction Reporter Array 21
2. 6. Immunocytochemistry 22
2. 7. Cell fractionation 22
2. 8. miRNA expression Arrays 23
2. 9. miR mimic and inhibitor transfection 24
2. 10. *In vivo* antitumor activity in xenograft model 24
2. 11. Immunohistochemistry of tumor tissues 25
2. 12. Statistical analysis 25
C. Results 26
1. The growth inhibitory activity and related cellular signaling of PsA in A549 lung cancer cells 26
2. PsA inactivates Hippo signaling pathway via modulation of the protein expression of LATS1 and YAP 30
3. PsA reduces colony formation and inhibits migration and invasion 33
4. PsA regulates apoptosis and proliferation 36
5. The effects of PsA on miRNA levels 38
6. The effects of miR-4485 mimic on cell migration, colony formation and invasiveness 41

7. The effects of miR-4485 inhibitor on cell migration, colony formation and invasiveness 44
8. Cytotoxic activity of PsA and its analogues 47
9. Antitumor effect of compound **30** in a tumor xenograft model 54
D. Discussion 57

Part III: Antimetastatic Effect of Halichondramide in PC3 Human Prostate Cancer Cells 59
A. Introduction 60
B. Materials and Methods 63
1. Materials 63
1. 1. Reagents and antibodies 63
1. 2. Compounds 63
1. 3. Cell culture 64
2. Methods 66
2. 1. The evaluation of antiproliferation activity 66
2. 2. Analysis of gene expression by Real-time RT-PCR 66
2. 3. Western blot analysis 68
2. 4. Wound healing assay 69
2. 5. Cell migration assay 69
2. 6. Gelatin zymography 70
2. 7. Statistical analysis 71
C. Results 72

1. Growth Inhibitory Activity of Halichondramide in PC3 Prostate Cancer Cells 72
2. Modulation of the Gene Expression Levels of PRL-3, MMPs, and Cadherins by HCA 75
3. Suppressive Expression of PRL-3 and Its Associated Proteins by HCA .. 76
4. Inhibitory Effect of HCA on Cell Migration and Invasion 78
5. Suppressive Effect of HCA on the MMPs in Gelatin Zymography 81
D. Discussion 83

Part IV: Conclusion..... 86

References 90
Abstract in Korean..... 108

List of Figures

Figure 1. Hippo signaling pathway 7

Figure 2. A model for the processing and mode of action of miRNA..... 9

Figure 3. Schematic diagram of the complex metastatic process..... 11

Figure 4. Chemical structure of psammaplin A 19

Figure 5. The growth inhibitory activity of PsA in A549 lung cancer cells ... 28

Figure 6. Inactivation of Hippo signaling pathway in the A549 cell line..... 31

Figure 7. The inhibitory effects of PsA on colony formation, cell migration and invasiveness 34

Figure 8. The effect of PsA on cell apoptosis and proliferation..... 37

Figure 9. Comparison of miRNA expression levels of PsA treated cells and parent cells 39

Figure 10. miR-4485 mimic inactivates the Hippo signaling pathway and modulates migration and invasion 42

Figure 11. miR-4485 inhibitor activates the Hippo signaling pathway and induces migration and invasion 45

Figure 12. Anti-proliferative activity of compound **30** in cultured human A549 lung cancer cells 53

Figure 13. Antitumor effect of compound **30** in a tumor xenograft model..... 56

Figure 14. The schematic diagram of PRL-3 and down-stream signaling pathway 62

Figure 15. Chemical structure of halichondramide 65

Figure 16. The growth inhibitory activity of HCA in PC3 prostate cancer cells 73

Figure 17. The effects of HCA on the mRNA expression of PRL-3 and its down-stream genes and metastatic biomarkers 75

Figure 18. The effects of HCA on the expression of PRL-3 and its associated proteins..... 77

Figure 19. The inhibitory effects of HCA on cell migration and invasion 79

Figure 20. The inhibitory effects of HCA on gelatin degradation..... 82

Figure 21. Overview of the mechanism of PsA and HCA..... 89

List of Tables

Table 1. Summary of Hippo signaling pathway 5

Table 2. Cytotoxic activity of PsA and its analogues..... 49

Table 3. Cytotoxic activity of PsA analogues..... 51

Table 4. The sequences of the primer pairs that were used to examine specific target genes in RT-PCR analysis 68

Part I: General Introduction

A. Background

1. Lung cancer

Lung cancer is the leading cause of cancer-related death as it is characterized by malignant tumors, accounting for one million deaths worldwide every year [1], and its incidence is increasing. The poor survival rate of patients is largely attributed to delayed diagnosis with local or advanced metastasis to distant organs [2]. Non-small-cell lung cancer (NSCLC) accounts for up to 80 % of all lung cancer cases. In recent years, great progress has been made in the field of molecular therapies for NSCLC. However, the long-term survival for lung cancer patients including those with NSCLC, is still unsatisfactory [3]. Therefore, the search for more useful biomarkers and therapeutic targets is still the demanding task.

2. Hippo signaling pathway

The Hippo signaling pathway, also known as the Salvador-Warts-Hippo pathway, was originally discovered in *Drosophila melanogaster* [4 5]. The core components of the pathway in the fly, including Hippo, Sav, Wts, Yki, and Mats, are highly conserved in mammals as Mst1/2, WW45, LATS1/2, YAP, and Mob1, respectively [5a, 6] (Figure 1). Recently, several studies have clearly shown the role of the Hippo pathway in controlling organ size and other biological processes including cell fate determination, mitosis and pluripotency [7]. YAP is a key effector protein in the Hippo pathway and is negatively regulated by the Mst1/2-LATS1/2-Mob1 complex through direct phosphorylation. The phosphorylation of YAP inhibits cell proliferation; therefore, impairment of the Hippo signaling pathway has been implicated in many human cancers including gastric cancer [8].

Although recent reports have identified upstream positive and negative regulators of the pathway [9], its membrane proximal components are yet to be established, although cell density and actin cytoskeletal organization can modulate this pathway [10]. Integrin-linked kinase (ILK) is an integrin associated, actin and tubulin cytoskeletal interacting effector, which regulates cell adhesion and integrin-mediated as well as growth factor regulated functions [11]. ILK coordinates several signaling pathways, and it has been shown to activate PI3K/Akt, Wnt, TGF-β and epithelial–mesenchymal transition signaling in various types of cancer cells [11]. Furthermore, ILK expression is upregulated in many types of cancers [11b, 12]. In a previous study conducted by another research group, it was demonstrated that ILK

is a critical negative regulator of the Hippo tumor suppressor pathway in human breast, prostate and colon cancer cells [13]. ILK prevents merlin dephosphorylation and activation, resulting in inhibition of the Hippo kinase cassette and nuclear accumulation of YAP. Inhibition of ILK expression with PsA, results in a dramatic activation of the Hippo pathway, leading to YAP phosphorylation and sequestration (retention) in the cytoplasm. These data collectively point to an important activity of PsA in inhibiting the Hippo tumor suppressor pathway in cancer cells, and identify PsA as a potential therapeutic target for lung cancer via regulation of the Hippo signaling pathway. The components of the Hippo signaling pathway are summarized in Table 1.

Table 1. Summary of Hippo signaling pathway

Drosophila melanogaster	Human ortholog(s)	Protein Description & Role in Hippo Signaling Pathway
Merlin (Mer)	**NF2**	FERM domain-containing apical protein that associates with Ex and Kibra as an upstream regulator of the core kinase cascade
Hippo (Hpo)	**MST1, MST2**	Sterile-20-type kinase that phosphorylates and activates Wts
Salvador (Sav)	**WW45 (SAV1)**	WW domain-containing protein that may act as a scaffold protein, facilitating Warts phosphorylation by Hippo
Warts (Wts)	**LATS1, LATS2**	Nuclear DBF-2-related kinase that phosphorylates and inactivates Yki
Mob as tumor suppressor (Mats)	**MOBKL1A, MOBKL1B**	Kinase that associates with Wts to potentiate its catalytic activity
Yorkie (Yki)	**YAP, TAZ**	Transcriptional coactivator that binds to Sd in its active, unphosphorylated form to activate expression of transcriptional targets that promote cell growth, cell proliferation, and prevent apoptosis
Scalloped	**TEAD1,**	Transcription factor that binds Yki to regulate

(Sd)	**TEAD2, TEAD3, TEAD4**	target gene expression

Abbreviations: NF2, Neurofibromin 2; MST, Macrophage-stimulating protein; SAV1, Protein salvador homolog 1; LATS, large tumor suppressor; MOBKL, Mps one binder kinase activator-like; YAP, Yes-associated protein; TAZ, Transcriptional coactivator with PDZ binding motif; TEAD, TEA domain family member.

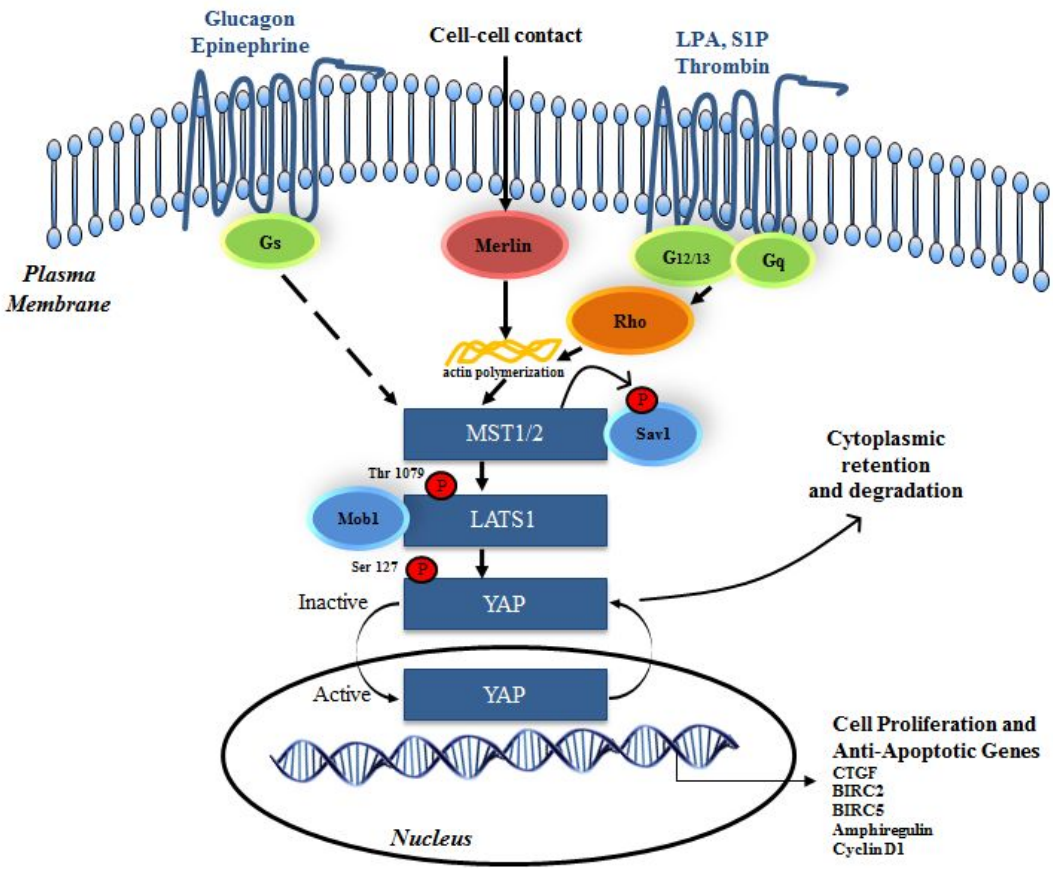

Figure 1. Hippo signaling pathway

Components of the pathway are conserved in mammals with MST1/2 playing the equivalent role to Hippo. Mst1/2 phosphorylates LATS1 and LATS1 phosphorylates YAP. When phosphorylated YAP is held in the cytoplasm bound to a 14-3-3 protein or degraded by the proteasome. When not phosphorylated, YAP moves into the nucleus to regulate the transcription of pro-proliferative and anti-apoptotic genes as a transcription coactivator. Upstream control of the Hippo pathway is by cell-cell interaction and G protein coupled receptors. Receptors coupled to G12/13 or Gq activate in a Rho and actin dependent manner while

receptors coupled to Gs inhibit.

3. MicroRNA

A new class of small non-coding RNAs, named microRNAs (miRNAs), were identified during the characterization of genes that control the timing of larval development in *Caenorhabditis elegans* [14]. Since then, other new members of this class were reported in viruses, plants and animals [15]. Besides their function in developmentally timed events, miRNAs are also implicated in a wide range of biological processes and their deregulation leads to diverse diseases [16]. Mature miRNAs are defined as small non-coding RNAs of ~22 nt that inhibit the expression of protein coding genes (Figure 2). Several models have been proposed to explain the exact mechanisms by which miRNAs regulate their target genes. In animals, miRNAs hinder the stability of messenger RNAs and their translation, binding preferably to their 3′ untranslated regions (UTRs) [17]. Whereas the interactions between miRNAs and their target genes in plants usually show a perfect complementarity, these interactions in animals often lead to imperfect base pairings. This is the reason why prediction of animal miRNA targets is a challenging task and has given rise to several miRNA target prediction algorithms. These programs provide good resources to find miRNAs or miRNA targets in relation to a particular experiment; however, concerns have been raised about their sensitivity and specificity [18]. Consequenyly, researchers often use putative miRNA targets of several prediction algorithms or an integration of these predictions [19].

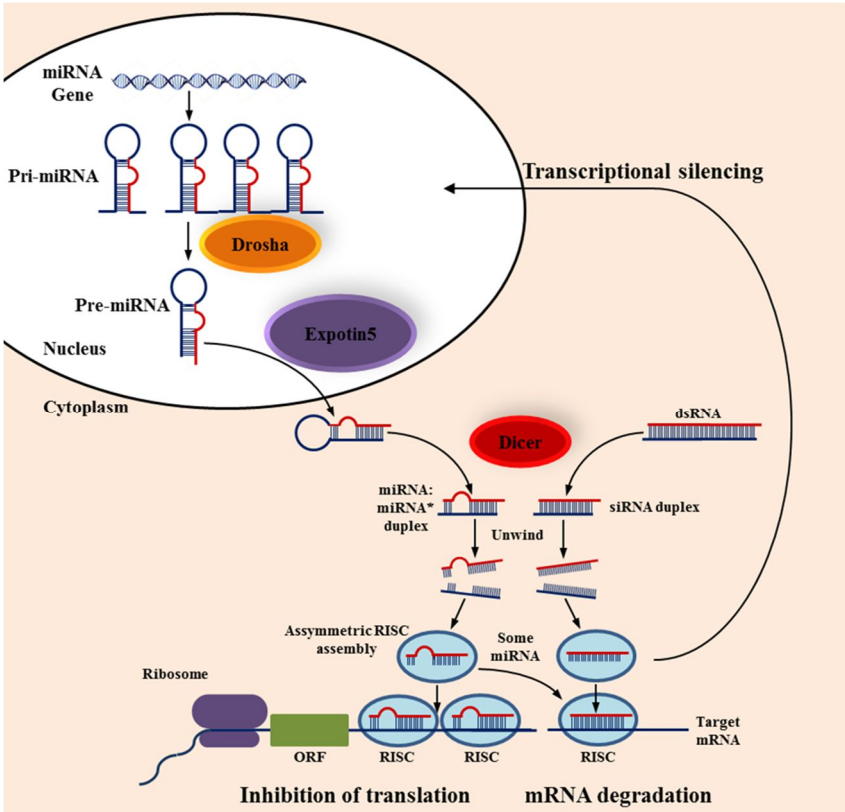

Figure 2. A model for the processing and mode of action of miRNA

This canonical maturation includes the production of the primary miRNA transcript (pri-miRNA) and cleavage of the pri-miRNA by the microprocessor complex (Drosha) in the nucleus. The resulting precursor hairpin, the pre-miRNA, is exported from the nucleus by Exportin-5. In the cytoplasm, the RNase Dicer in complex cleaves the pre-miRNA hairpin to its mature length. The functional strand of the mature miRNA is loaded into the RNA-induced silencing complex (RISC), where it guides RISC to silence target mRNAs through mRNA cleavage, translational repression.

4. Cancer metastasis and epithelial-mesenchymal transition

Metastases are the main cause of 90% of human cancer deaths [20]. A characteristic of metastasizing cells is their transition from an epithelial to a mesenchymal state; the process is known as epithelial-mesenchymal transition (EMT) [21] (Figure 3). EMT is involved in embryonic development and cancer progression. In EMT, the loss of epithelial functions, such as cell–cell contact, cytoskeletal remodeling, and polarity changes are complemented by acquisition of mesenchymal functions, resulting in increased cell motility and invasion. Loss of expression of epithelial-specific proteins, such as E-cadherin, and increased expression of mesenchymal-specific proteins, such as vimentin, can be used as markers of EMT [22]. During tumor progression, cancer cells can acquire motility and invasive ability by initiating an EMT process, which can potentially lead to distant metastases [23]. Recent evidence indicates that EMT is a critical step in cancer cell invasion and metastasis and that it positively correlates with poor prognosis in cancer patients [24]. Previous reports noted that cells at early stages cancers have an epithelial-like phenotype, whereas cells from advanced cancerous lesions have a more mesenchymal-like phenotype [25].

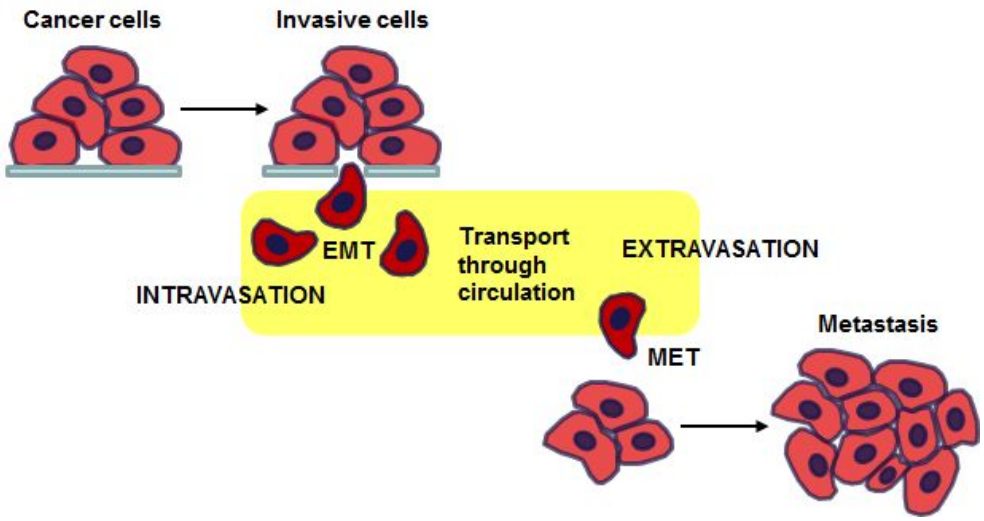

Figure 3. Schematic diagram of the complex metastatic process

Epithelial–mesenchymal transition (EMT) alters the cell phenotype to allow intravasation into the systemic circulation. Mesenchymal–epithelial transition (MET) occurs at the site of distant metastases.

B. The Purpose of This Study

Based on the importance of identifying bioactive natural compounds in cancer treatment, the present study attempts to discover novel mechanisms of action of PsA and HCA.

PsA, a natural product from marine sponge, is well acknowledged for its possible roles as a histone deacethylase inhibitor [26], and recently studies have shown that one of the PsA analogue has antitumor effects in *in vivo* models in A549 human lung cancer cells [27]. However, the biological function of PsA, and its possible use as an antitumor agent for human lung cancer, is unknown. Several studies have revealed the importance of the novel Hippo tumor-suppressor pathway in regulating cell proliferation, apoptosis and tumorigenesis. Therefore, the purpose of the present study was to investigate the biological function of PsA in human lung cancer cells and to elucidate whether PsA regulates the Hippo signaling pathway.

HCA, a trisoxazole-containing macrolide isolated from the marine sponge *Chondrosia corticata* has been known to exhibit cytotoxicity and antifungal activities. In previous studies, HCA was also found to exhibit antiproliferative activity against a variety of cancer cells. However, the precise mechanism of action of HCA as an antitumor agent remains to be elucidated.

In the present study, it was proven that PsA modulates the Hippo signaling pathway in A549 human lung cancer cells in *in vitro* model and inhibits lung

cancer tumors in *in vivo* model. In addition, HCA was also found to exhibit antimetastatic activity in the highly metastatic PC3 human prostate cancer cells. Thus, these two bioactive compounds from marine natural product may serve as possible therapeutic agents to treat cancer.

Part II: Antitumor Activities of Psammaplin A and its Analogues in A549 Human Lung Cancer Cells

A. Introduction

Psammaplin A (PsA) was originally independently isolated by several different research groups from the *Psammaplysilla* sponge or unidentified sponges in 1987 [28]. PsA has a unique symmetrical structure of disulfide dimers derived from bromotyrosine. Biological activity studies have revealed that PsA has various bioactivities such as antimicrobial activity [29], cytotoxicity against the leukemia cell line P388 [28a, 30], and inhibition of DNA gyrase [29], DNA topoisomerase [31], farnesyl protein transferase [32], and leucine aminopeptidase [32]. Additionally, PsA activates PPARγ and induces apoptosis in human breast cancer cells [33]. PsA was also shown to be a potent inhibitor of both DNA methyltransferase (DNMT) and histone deacetylase (HDAC) [26b, 34]. Histone deacetylase inhibitors (HDACi) are candidates for treatment of cancer. HDACi suppress the progression of tumorigenesis through epigenetic regulation of acetylation of target proteins such as transcription factors, chaperones, signaling transduction molecules, and DNA repair proteins [35]. HDACi also regulate the expression of several genes involved in the angiogenesis signaling pathway [36]. Indeed, several HDACi are undergoing clinical trials, and some compounds including vorinostat (SAHA) and romidepsin (FK-228) have already been approved by the U.S. FDA, as cancer chemotherapeutic agents for cutaneous T-cell lymphoma therapy [37]. Moreover, several potent synthetic HDACi were also recently been reported [38]. Recently, the Shin group, one of our research collaborators, also isolated PsA from an unidentified sponge collected from the southern region of Korea, and confirmed its significant cytotoxicity against the

leukemia cell line as reported in previous studies [32]. Although the biological activities of PsA are promising, the presence of PsA in marine natural products is very low. Therefore, one of research collaborators aimed to develop very efficient methods for the synthesis of PsA and its analogues. To overcome such shortcomings, a new efficient and concise synthetic method of PsA was developed. Employing the new efficient synthetic method, a structure-activity relationship study utilizing the more diverse analogues of PsA was attempted to procure the potentially tumor active compounds. Here, a novel cellular mechanism of action of PsA in A549 human lung cancer cells and a structure-activity relationship (SAR) study of PsA analogues were demonstrated. In addition to the above mentioned objectives, antitumor activity of a selected compound was evaluated and compared with those of PsA. In addition, selected compound was evaluated for underlying molecular mechanism of the growth inhibitory activity on human lung cancer cells, and *in vivo* antitumor activity in the A549 human lung cancer cell-implanted mouse xenograft models.

B. Materials and Methods

1. Materials

1. 1. Reagents and antibodies

RPMI 1640 medium, fetal bovine serum (FBS), antibiotic-antimycotic solution, trypsin-EDTA, TRI reagent, Alexa Fluor 488-labeled donkey anti-goat IgG, Opti-MEM Reduced Serum Medium, and Lipofectamine RNAiMAX were purchased from Invitrogen (Grand Island, NY, USA). Bovine serum albumin (BSA), sulforhodamine B (SRB), trichloroacetic acid and other agents unless otherwise indicated were purchased from Sigma-Aldrich (St. Louis, MO, USA). miR-4485 specific mimic and inhibitor, negative control miRNA were purchased from Bioneer (Daejeon, Korea). Antibodies against YAP, anti-phospho-LATS1, and anti-phospho-YAP, and anti-GAPDH were obtained from Cell Signaling Technology (Danvers, MA, USA). β-actin were obtained from Santa Cruz Biotechnology (Santa Cruz, CA, USA). DAPI was purchased from Vector Laboratories (Burlingame, CA, USA). Complete protease inhibitor cocktail and phosphatase inhibitor cocktail were purchased from Roche Applied Science (Penzberg, Germany). Cignal Finder Signal Transduction 45-Pathway Reporter Array™ was purchased from QIAGEN (Redwood City, CA, USA). BD Pharmingen™ BrdU Flow Kits were purchased from BD Biosciences (San Jose, CA, USA).

1. 2. Compounds

Psammaplin A (PsA) was isolated from an unidentified sponge collected from the southern region of Korea, as described previously [32] (Figure 4). Although the biological activities of PsA are promising, the abundance of PsA in marine natural products is very low. Therefore, very efficient methods for the synthesis of PsA and its analogues were developed by our research collaborator and the synthetic compounds were kindly provided.

1. 3. Cell culture

The human lung carcinoma A549 cells were provided by the Korean Cell Line Bank (Seoul, Korea). The cell line was cultured in RPMI 1640 medium supplemented with 10% FBS and antibiotics-antimycotics (PSF; 100 units/mL penicillin G sodium, 100 μg/mL streptomycin, and 250 ng/mL amphotericin B). The cells were incubated at 37°C and 5% CO_2 in a humidified atmosphere.

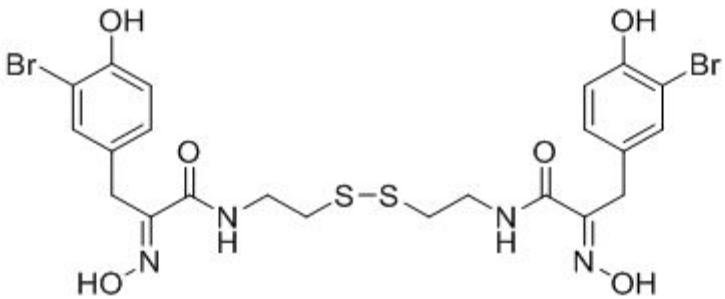

Figure 4. Chemical structure of psammaplin A

2. Methods

2. 1. Cell proliferation assay

The cells ($3 - 4 \times 10^4$ cells/ml) were treated with various concentrations of compounds in 96-well culture plates. After 72 h of treatment, the cells were fixed with 10% TCA solution, and the cell proliferation was determined through a sulforhodamine B (SRB) assay. The percentage of cell proliferation was determined according to the following formula: cell proliferation (%) = $100 \times \{(A_{treated} - A_{zero\ day})/(A_{control} - A_{zero\ day})\}$, where A is the average absorbance. The IC_{50} values were calculated through non-linear regression analysis using TableCurve 2D v5.01 (Systat Software Inc., San Jose, CA, USA).

2. 2. Western blot

For western blot analysis, cells were lysed through boiling in 2× sample loading buffer (250 mM Tris-HCl pH 6.8, 4% SDS, 10% glycerol, 0.006% bromophenol blue, 2% β-mercaptoethanol, 50 mM sodium fluoride, and 5 mM sodium orthovanadate) and further incubated for 5 min at 100℃. Equal amounts (10 or 50 μg) of protein were subjected to 10-14% SDS-PAGE and transferred onto PVDF membranes (Millipore, Bedford, MA, USA). The blots were blocked with 5% bovine serum albumin (BSA) in Tris-buffered saline containing 0.1% Tween-20 (TBST) for 1 h at room temperature, and then incubated with primary antibodies in 2.5% BSA in TBST overnight at 4°C. The membranes were washed three times with TBST and incubated with the corresponding secondary antibodies diluted in

2.5% BSA in TBST for 2 h at room temperature. After washing three times with TBST, the membranes were exposed to enhanced chemiluminescence (ECL) solution (Intron, Daejeon, Korea). The blots were detected with an LAS-4000 (Fuji Film Corp., Tokyo, Japan).

2. 3. Detection of apoptosis

The Annexin V-FITC and propidium iodide flow kit (BD Biosciences, CA, USA) was used according to manufacturer's instructions. Briefly, the translocation of phosphatidylserine residues from the inner to the outer side of plasma membrane was assessed by FITC-conjugated Annexin-V staining. A549 cells were stained 24 hours after addition of PsA. After co-staining with propidium iodide cells were analyzed by FACSCalibur flow cytometer (BD Biosciences, CA, USA).

2. 4. Measuring cell proliferation

The bromodeoxyuridine (BrdU) flow kit (BD Biosciences, CA, USA) was used according to the manufacturer's instructions for cell cycle analysis. Briefly, A549 cells were analyzed 24 hours after treatment of PsA. To label proliferating cells, cells were incubated with 10 μM BrdU for 1 hour prior to harvesting and fixation in 70% cold ethanol. Surface staining carried out followed by staining for BrdU. 7-AAD was used for total DNA staining. Analysis was performed on flow cytometer and the percentage of BrdU positive cells was calculated.

2. 5. Signal Transduction Reporter Array

The Cignal Finder Signal Transduction 45-Pathway Reporter Array™ (QIAGEN, CA, USA) was used per the manufacturer's instructions. A549 cells were plated in the Cignal 45-pathway reporter assay 96-well plate format for reverse transfection. After 24 hours of transfection, the medium was replaced with full growth medium cells were treated with PsA for 24 hours. To test various cellular signaling responses to PsA, the activities of transcription factors were quantified by using the Dual-Luciferase Reporter Assay System (QIAGEN, CA, USA).

2. 6. Immunocytochemistry

Cells were grown on cover slips in dishes. After treatment, the cells were fixed with 4% paraformaldehyde (in PBS) for 15 min. The fixed cells were blocked with 1% BSA (in PBS) containing 0.1% Triton X-100 (permeabilizing condition) or without Triton X-100 (non-permeabilizing condition) for 30 min at room temperature. The cells were incubated with primary antibody at 4°C overnight. Following the overnight incubation, the cells were incubated with donkey anti-goat secondary antibody conjugated to Alexa 594 (Invitrogen) for 2 h at room temperature. DAPI (0.5 μg/ml) was used to counterstain the nuclei. The images were obtained using a Zeiss ApoTome microscope (Carl Zeiss, Jena, Germany).

2. 7. Cell fractionation

The cells were washed with ice-cold PBS three times and then washed once rapidly with cold fractionation lysis buffer (20 mM Tris-Cl pH 7.4, 100 mM NaCl, 2 mM MgOAc, 5 mM KCl, 10 μM GTP, and protease inhibitor). The scraped cells

in lysis buffer were incubated on ice for 10 min and then lysed by passing through a 27-gauge needle 35 times on ice. Small amounts of the total lysate samples were reserved from the lysates, and the remaining samples were centrifuged (20 min, 2 000 rpm, 4°C). The supernatant was then collected and centrifuged (30 min, 14 000 rpm, 4°C). After the second centrifugation, the resulting supernatant was kept for analysis of the cytosolic fraction, and the pellet was washed with lysis buffer for membrane fraction extraction. The lysis buffer was removed by centrifugation (20 min, 14 000 rpm, 4°C), and the membrane pellet was once again washed with ice-cold PBS. After removal of PBS (5 min, 14 000 rpm, 4°C), the membrane pellet was suspended in 1% NP-40 lysis buffer for 1 h on ice with mixing every 10 min. The total, cytosolic and membrane lysates were boiled with 2× Laemmli sample buffer at 95°C for 10 min.

2. 8. miRNA expression Arrays

For the quality control, RNA purity and integrity were evaluated by OD 260/280 ratio, and analyzed by Agilent 2100 Bioanalyzer (Agilent Technologies, Palo Alto, USA). The Affymetrix Genechip miRNA 4.0 array process was executed according to the manufacturer's protocol. 1000ng RNA samples were labeled with the FlashTag™ Biotin RNA Labeling Kit (Genisphere, Hatfield, PA, USA). The labeled RNA was quantified, fractionated and hybridized to the miRNA microarray according to the standard procedures provided by the manufacture. The labeled RNA was heated to 99°C for 5 minutes and then to 45°C for 5 minutes. RNA-array hybridization was performed with agitation at 60 rotations per minute for 16 hours

at 48°C on an Affymetrix® 450 Fluidics Station. The chips were washed and stained using a Genechip Fluidics Station 450 (Affymetrix, Santa Clara, California, United States). The chips were then scanned with an Affymetrix GCS 3000 canner (Affymetrix, Santa Clara, California, United States). Signal values were computed using the Affymetrix® GeneChip™ Command Console software. The comparative analysis between test sample and control sample was carried out using fold-change. All Statistical test and visualization of differentially expressed genes was conducted using R statistical language v. 3.1.2.

2. 9. miR mimic and inhibitor transfection

For transient transfection, cells were transfected with 20 – 40 nM miR-4485 mimic and inhibitor using Lipofectamine RNAi MAX (Life) according to the manufacturer's instructions. *pcDNA3* vector and *pcDNA3-AXL* were kindly provided by Dr. Shuang-En Chuang (Institute of Cancer Research, National Health Research Institutes, Taiwan)

2. 10. *In vivo* antitumor activity in xenograft model

Six week-old male athymic mice (BALB/c nu/nu) were purchased Central Lab. Animal Inc. (Seoul, Korea). A549 cell suspension (1 x 10^7 cells in 0.1 mL of RPMI) was injected subcutaneously into the right flank of each mouse on day 0. The mice were treated when their tumor volume reached 50–60 mm^3. The animals were randomly divided into five groups (six animals per group). Compound **30** (15 or 30 mg/kg body weight), psammplin A (30 mg/kg body weight) dissolved in 0.05%

tween-80 in 0.9% NaCl was administered intraperitoneally three times a week. The positive control group was treated with paclitaxel (5 mg/kg body weight), and the negative control group was treated with an equal volume of the vehicle. The tumor volume was monitored two times per week for 35 days using calipers and estimated using the following formula: tumor volume (mm^3) = (width) x (length) x (height) x π /6. The body weight of each mouse was also monitored for toxicity.

2. 11. Immunohistochemistry of tumor tissues

The immunohistochemical analysis of tumor tissues was conducted to detect cell proliferation biomarkers using the Ki-67. Sections of the tumor tissues were incubated at 4 °C overnight with the antibodies for Ki-67, detected using the EnVision Plus/HRP detection system (Dako, Carpinteria, CA, USA), and counterstained with hematoxylin and eosin. The stained section was observed under an inverted phase-contrast microscope and photographed.

2. 12. Statistical analysis

The data are presented as the means ± SD for the indicated number of independently performed experiments. The statistical significance ($p < 0.05$) was assessed using Student's *t*-test. All statistical tests were two-sided.

C. Results

1. The growth inhibitory activity and related cellular signaling of PsA in A549 lung cancer cells

Antiproliferative potential of psammaplin A (PsA) in A549 human lung cancer cells was evaluated using the sulforhodamine B (SRB) assay. As illustrated in Figure 5A, PsA exhibited antiproliferative activity against A549 cells in a concentration-dependent manner, and the IC_{50} value was 1.18 μM for an incubation of 72 h. Specifically, PsA treatment at the 2 μM concentration produced remarkable decrease in cell numbers (Figure 5B), and the cells also become shrunken and sharp in shape, suggesting that HCA might exhibit cytostatic effect at relatively low concentrations but exert a cytotoxic effect at higher concentrations.

To determine the change in the form of bringing the cells in this cytotoxicity was (Figure 5B), it was confirmed that induces death of the cells (Figure 5C). Promoter activity assay was performed to determine how different intracellular signaling pathways were involved in the above mentioned cellular events. It was found that PsA effectively suppressed the PI3K/Akt pathway among the various signaling pathways (Figure 5D). These effects of PsA were confirmed by western blot analysis, it was also confirmed that the amounts of p101 and phosphorylated proteins of p85 and p50 (subunits of PI3K) were reduced (Figure 1E). A recent study exploring the relation among Integrin-linked kinases (ILK), PI3K and Akt, demonstrated that ILK could modulate the Hippo signaling pathways. This

information suggests that PsA might regulate Hippo signaling pathway via downregulation of ILK (Figure 1F).

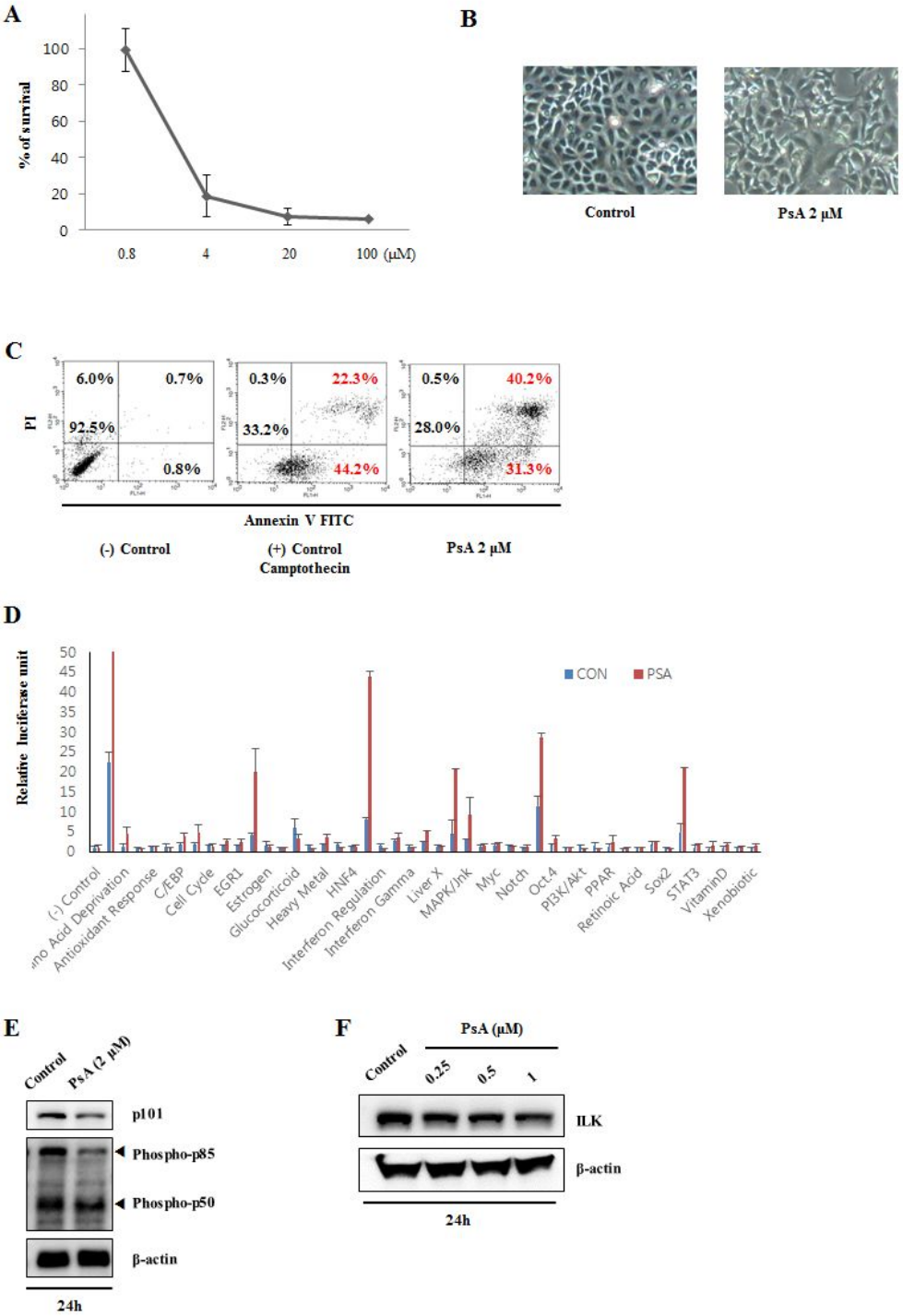
A
% of survival
100
80
60
40
20
0
0.8
4
20
100 (μM)
B
Control
PsA 2 μM
C
PI
6.0%
0.7%
92.5%
0.8%
0.3%
22.3%
33.2%
44.2%
0.5%
40.2%
28.0%
31.3%
Annexin V FITC
(-) Control
(+) Control
Camptothecin
PsA 2 μM
D
Relative Inciferase unit
CON
PSA
(-) Control
Antioxidant Response
C/EBP
Cell Cycle
EGR1
Estrogen
Glucocorticoid
Heavy Metal
HNF4
Interferon Regulation
Interferon Gamma
Liver X
MAPK/Jnk
Myc
Notch
Oct4
PI3K/Akt
PPAR
Retinoic Acid
Sox2
STAT3
VitaminD
Xenobiotic
E
Control
PsA (2 μM)
p101
Phospho-p85
Phospho-p50
β-actin
24h
F
PsA (μM)
Control
0.25
0.5
1
ILK
β-actin
24h

Figure 5. The growth inhibitory activity of PsA in A549 lung cancer cells

(A) A549 cells (3.5×10^4 cells/mL) were treated with PsA for 72 h; subsequently, anti-proliferative activity was determined by the SRB protein dye method as described in the Method Section. (B) The morphological changes of A549 cells treated with PsA for 24 h were observed under a phase-contrast microscope and photographed. (C) Detection of apoptotic cell population by annexin V-FITC and PI double staining method. (D) Inhibition of PI3K/Akt pathway was determined by Cignal Finder Signal Transduction 45-Pathway Reporter Array™. (E and F) Cells were treated with PsA for the indicated times and concentrations. The lysates were analyzed by western blot analysis with antibody against p101, phospho-p85, phospho-p50 and ILK using β-actin as a loading control.

2. PsA inactivates Hippo signaling pathway via modulation of the protein expression of LATS1 and YAP

To test regulatory effects of PsA on Hippo signaling pathway, the signaling proteins expression were measured by western blot analysis. Large Tumor Suppressor 1 (LATS1) and Yes-associated protein (YAP) of the phosphorylated form increased following 24-hour PsA treatment those proteins were found to be dose-dependently increased (Figure 6A) and persisted even when the treatment duration was short (1 h ~ 4 h) (Figure 6B). In particular, the concentration-dependent increase in phosphorylated YAP was reflected by its raised amount in the cytoplasm (Figure 6C and 6D).

To explore the underying mechanisms involved I studied whether PsA affected the expression of phospho-LATS1 and phospho-YAP, which were involved in modulation of Hippo signaling pathway. E-cadherin expression in cancer cells is associated with cancer progression, invasion, metastasis, and cytoskeletal rearrangement. Expression of both the phospho-LATS1 and phospho-YAP were significantly upregulated in PsA treated cells in comparison to the control cells.

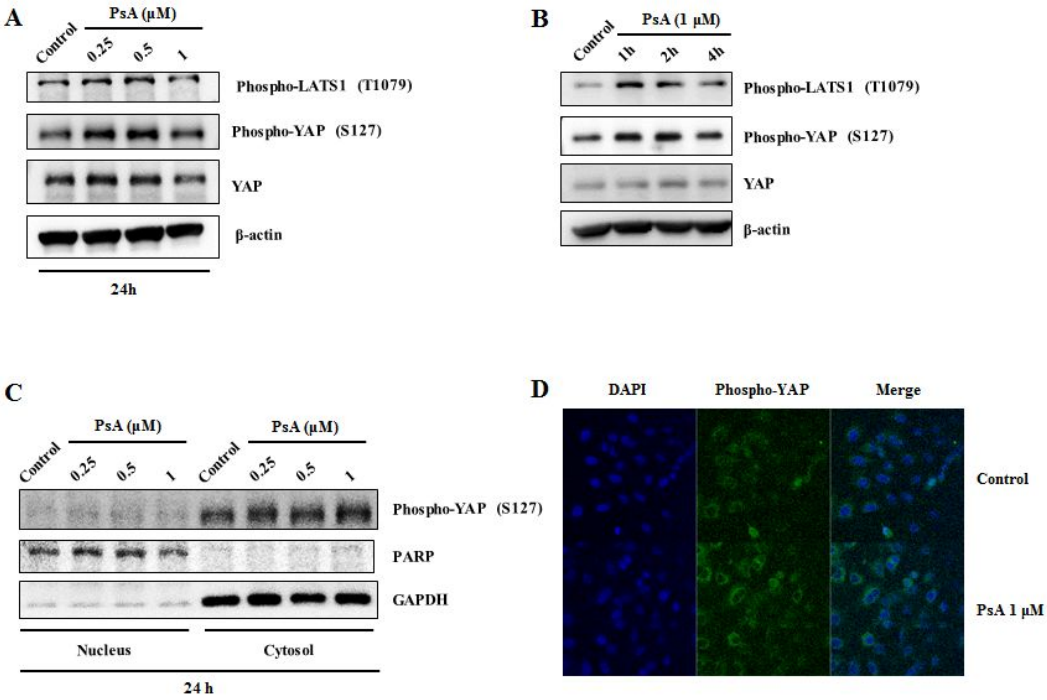
A
PsA (μM)
Control
0.25
0.5
1
Phospho-LATS1 (T1079)
Phospho-YAP (S127)
YAP
β-actin
24h
B
PsA (1 μM)
Control
1h
2h
4h
Phospho-LATS1 (T1079)
Phospho-YAP (S127)
YAP
β-actin
C
PsA (μM)
PsA (μM)
Control
0.25
0.5
1
Control
0.25
0.5
1
Phospho-YAP (S127)
PARP
GAPDH
Nucleus
Cytosol
24 h
D
DAPI
Phospho-YAP
Merge
Control
PsA 1 μM

Figure 6. Inactivation of Hippo signaling pathway in the A549 cell line

(A and B) Cells were treated with PsA for the indicated times and concentrations. The lysates were analyzed by western blot analysis with antibody against LATS1 and YAP using β-actin as a loading control. (C) Cells were treated with PsA for 24 h, and the cells were then harvested and fractionated into cytosolic and nucleic fractions. The each lysates were subjected to western blot using anti-phospho-YAP. GAPDH served as a cytosol marker and PARP served as a nucleus marker. (D) Cells treated with PsA for 24 h were subjected to immunocytochemistry. The cells were stained with phospho-YAP and DAPI.

3. PsA reduces colony formation and inhibits migration and invasion

To further demonstrate the role of PsA in lung tumorigenesis, and growth control activities of the PsA-treated cells were assessed. As expected, PsA-treated cells significantly reduced the colony formation in comparison to the control cells (Figure 7A). In comparison to well-developed colonies observed in control cells, PsA-treated cell colonies were fewer and relatively smaller in size (Fig. 7A). As shown in Figure 7B, PsA treated A549 human lung cancer cells exhibited significant inhibition of their migration ability in comparison to the control cells. In a wound-healing assay, a slower migration rate was demonstrated in PsA-treated group in A549 as compared with control cells. To determine whether treatment with PSA decreases invasion in a tumor-like context, we evaluated invasion of human lung cancer cells through Matrigel™ matrix in trans-wells assays with a collagen type I matrix (Figure 7C). As expected, the number of invasive cells were significantly reduced.

PsA-treated cells affected both migratory and invasive behavior of the cells PsA severely reduced the migration of A549 cells in a wound-healing assay (Figure 7B). Therefore, these results suggest that PsA is critical in suppressing the oncogenic property of A549 lung cancer cells.

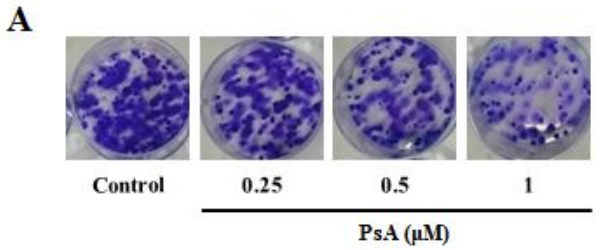
A
Control
0.25
0.5
1
PsA (μM)

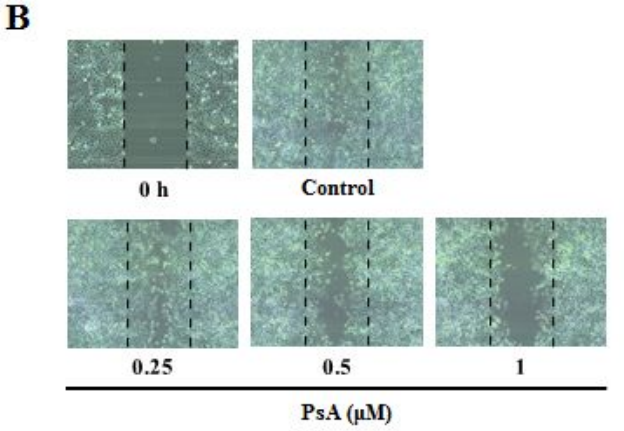
B
0 h
Control
0.25
0.5
1
PsA (μM)

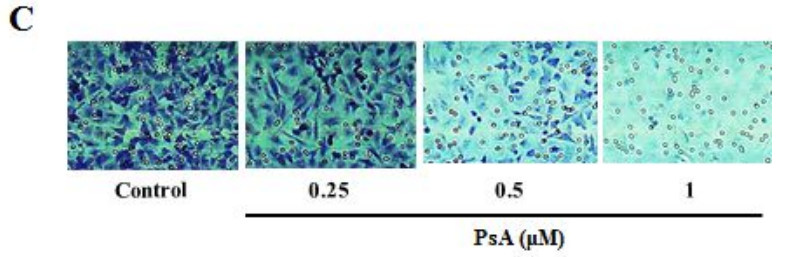
C
Control
0.25
0.5
1
PsA (μM)

Figure 7. The inhibitory effects of PsA on colony formation, cell migration and invasiveness

(A) PsA-treated cells were subjected to a colony formation assay. Representative pictures for colony growth are shown. Typical cell colonies observed by bright-field microscopy at day 14 after PsA treatment. (B) Migration in PsA treated cells was evaluated using wound healing assays. Images were captured at time 0 and 24 h after wounding. (C) A549 cells were either untreated or treated with PsA for 24 h and subjected to Matrigel-based transwell invasion assays. Invasive cells are imaged in a bright-field microscope.

4. PsA regulates apoptosis and proliferation

To determine whether PsA also decreased cell survival by induction of apoptosis, A549 cells were cultured with PsA at different concentrations (0.25, 0.5 and 1 μM) for 24 h and then assessed with Annexin V-FITC/PI double staining assay. As shown in Figure 8A, cells in the lower left quadrant were negative for both Annexin V-FITC and PI; cells in the lower right, positive for Annexin V-FITC, which indicated cells were in the early stages of apoptosis; cells in the upper left, positive for PI only, which indicated the dead cells; and cells in the upper right, positive for both Annexin V-FITC and PI, which indicated that the cells in the later stage of apoptosis or necrosis. The values indicated in the quadrants show the percentage of cells positive for both Annexin V-FITC and PI or Annexin V-FITC, separately. The results showed that the PsA treatment increased the percentage cells in the early stages of apoptosis and in the late stage of apoptosis (stained for Annexin V-FITC only and both Annexin V-FITC and PI, respectively) from 0.0%, 0.1% in the control group to 32.9%, 4.1% in PsA-treated group (1 μM), repectively.

Next, to assess if the proliferative capacity of A549 changed under PsA treatment conditions the percentage of proliferative cells was quantified by incorporation of the thymidine analog BrdU and FACS analysis (Figure 8B). Approximately 32.24% of the cells incorporated BrdU in the control group. The percentage of BrdU-positive cells decreased in a dose-dependently by PsA treatment. 23.19% of the cells were labeled with BrdU at the highest concentration (1 μM).

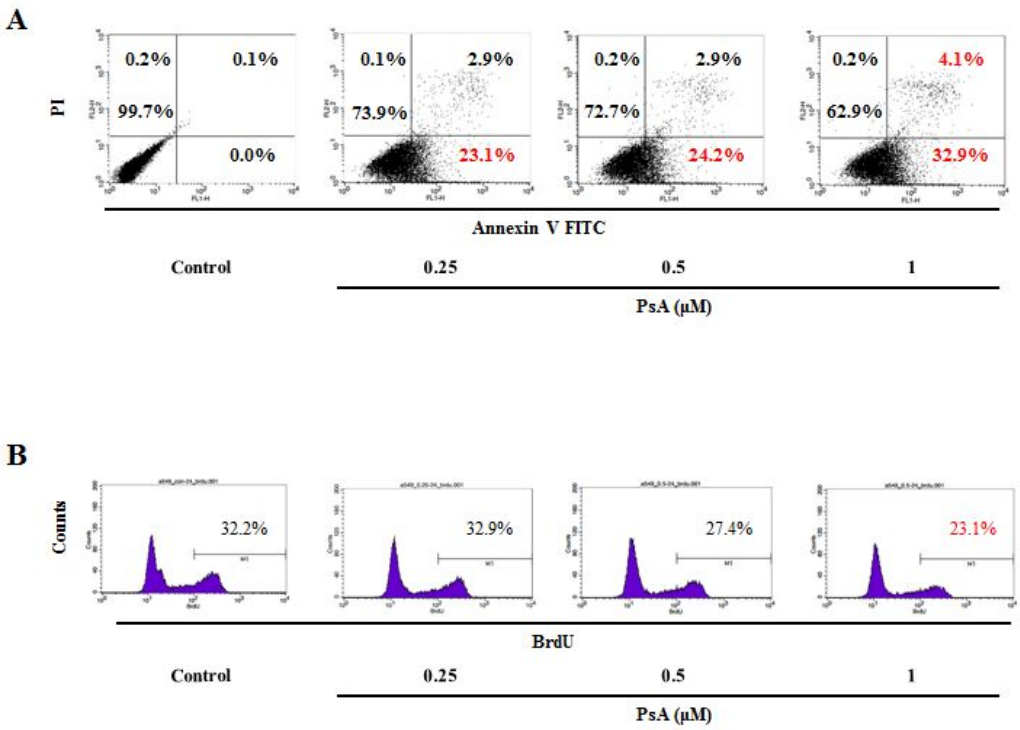

Figure 8. The effect of PsA on cell apoptosis and proliferation

(A) Evaluation of apoptosis by Annexin V-FITC/PI double staining assay and flow cytometer analysis after PsA treatment (0.25, 0.5, 1 μM) for 24 h. (B) Cells were treated with indicated concentrations of PsA. The visualization of BrdU uptake in individual cell populations of the suppression assay using flow cytometer.

5. The effects of PsA on miRNA levels

It has been reported that microRNA, a newly identified cellular regulator, binds to the 3'UTR (untranslated region) of the mRNA (Messenger RNA) and causes degradation of the target mRNA. In order to determine the miRNA expression profile of PsA-treated A549 cells, the expression levels of various miRNAs were determined by using Affymetrix Inc. miRNA 4.0 tool. Surprisingly, among the diffrentially expressed miRNAs miR-4485 was found to be highly expressed in PsA-treated cells (Figure 9).

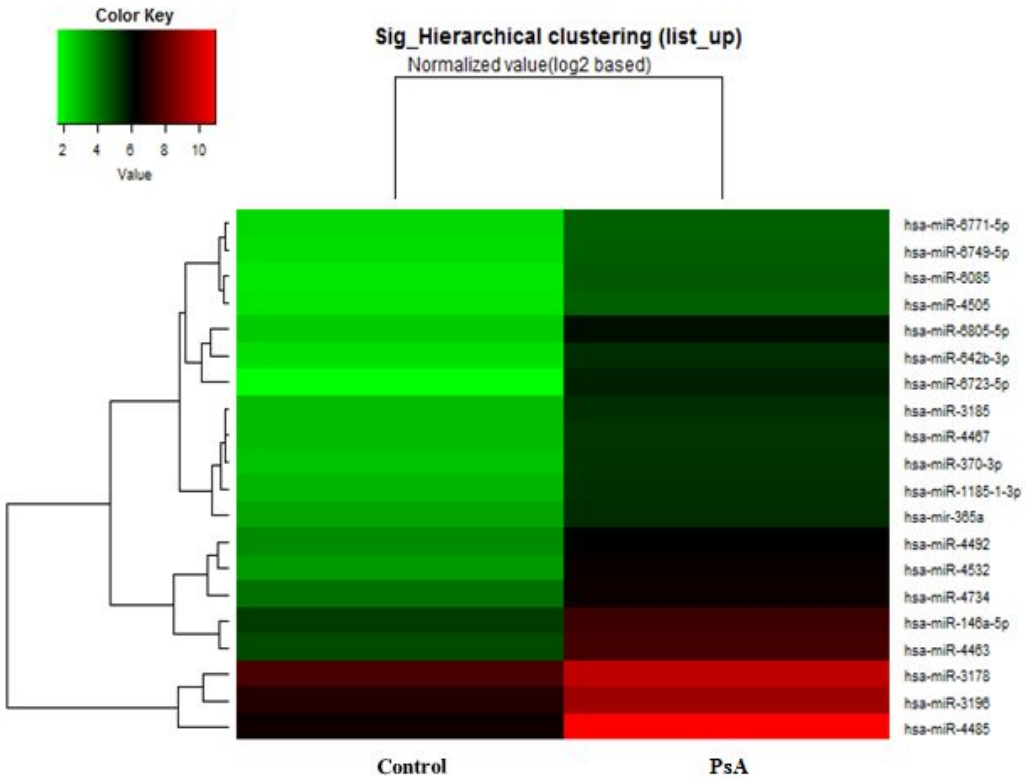
Color Key
2
4
6
8
10
Value
Sig_Hierarchical clustering (list_up)
Normalized value(log2 based)
hsa-miR-6771-5p
hsa-miR-6749-5p
hsa-miR-6085
hsa-miR-4505
hsa-miR-6805-5p
hsa-miR-642b-3p
hsa-miR-8723-5p
hsa-miR-3185
hsa-miR-4467
hsa-miR-370-3p
hsa-miR-1185-1-3p
hsa-mir-365a
hsa-miR-4492
hsa-miR-4532
hsa-miR-4734
hsa-miR-146a-5p
hsa-miR-4463
hsa-miR-3178
hsa-miR-3196
hsa-miR-4485
Control
PsA

Figure 9. Comparison of miRNA expression levels of PsA treated cells and parent cells

Hierarchical clustering analysis based on expression data for the 40 up-regulated miRNAs. Heatmap showing miRNAs with significant expression changes in PsA treated cells. Hierarchical clustering analysis was used to identify patterns of miRNA expression. Red signifies an increase in expression and green, a decrease in expression.

6. The effects of miR-4485 mimic on cell migration, colony formation and invasiveness

To further explore the significance and cellular role of miR-4485, we conducted gain-of-function and loss-of-function experiments. After treatment with the agonist of miR-4485 (mimic), phosphorylated LATS1 and YAP was significantly increased, similar results were shown in Figure 6 (Figure 10A). The miR-4485 mimic affected colony formation, migration and invasion. Colony formation assays also showed that miR-4485 reduced A549 cell proliferation (Figure 10B), which is consistent with PsA-treated results. As shown in Figure 10C and 10D, miR-4485 mimic transfected A549 cells exhibit significant inhibition of their migration and invasion ability compared with the controls.

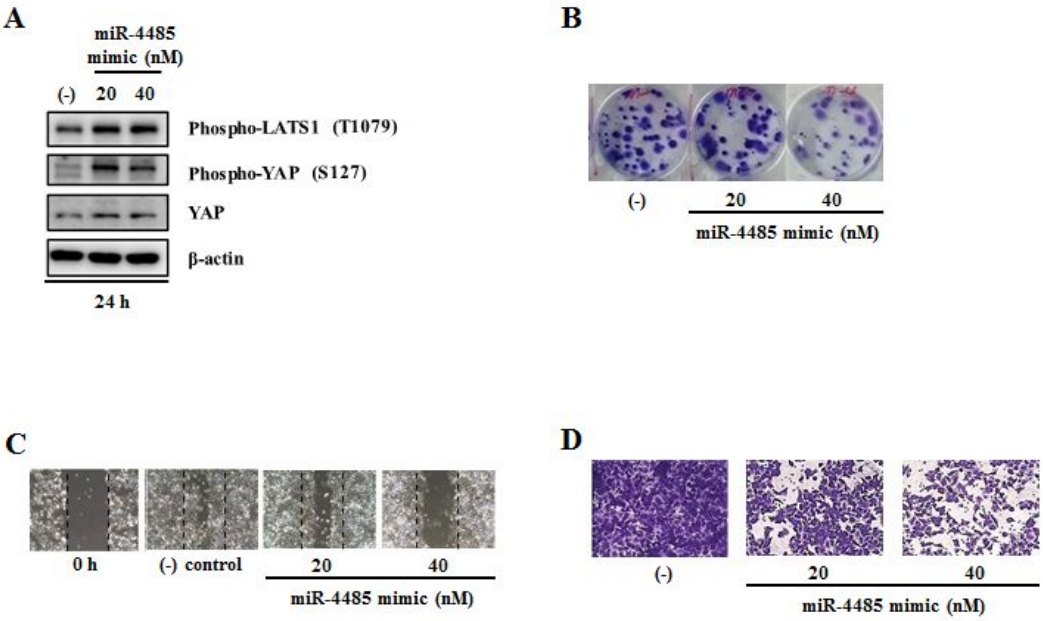
A
miR-4485
mimic (nM)
(-) 20 40
Phospho-LATS1 (T1079)
Phospho-YAP (S127)
YAP
β-actin
24 h
B
(-) 20 40
miR-4485 mimic (nM)
C
0 h
(-) control
20
40
miR-4485 mimic (nM)
D
(-)
20
40
miR-4485 mimic (nM)

Figure 10. miR-4485 mimic inactivates the Hippo signaling pathway and modulates migration and invasion

(A) Cells were treated with miR-4485 mimic for 24 h with indicated concentrations. The lysates were analyzed by western blot analysis with antibody against LATS1 and YAP using β-actin as a loading control. (B) The mimic treated cells were subjected to a colony formation assay. Representative pictures for colony growth are shown. Typical cell colonies observed by bright-field microscopy at day 14 of growth. (C) Migration in miR-4485 mimic treated cells was evaluated using wound healing assays. (D) A549 cells were either untreated or treated with the mimic for 24 h and subjected to Matrigel-based transwell invasion assays. Invasive cells are imaged in a bright-field microscope.

7. The effects of miR-4485 inhibitor on cell migration, colony formation and invasiveness

To test the above assumption, the analyses of loss-of-function of miR-4485 were performed. After transferring a miR-4485 inhibitor into A549 cells to reduce miR-4485, proteins level of phosphorylated LATS1 and YAP was decreased (Figure 11A). Compared with colonies observed in negative control cells, the miR-4485 inhibitor strongly promoted A549 cell proliferation (Figure 11B). The miR-4485 inhibitor transfected A549 cells exhibited significant increase in their migrating and invasive abilities compare with the negative controls (Figure 11C and 11D).

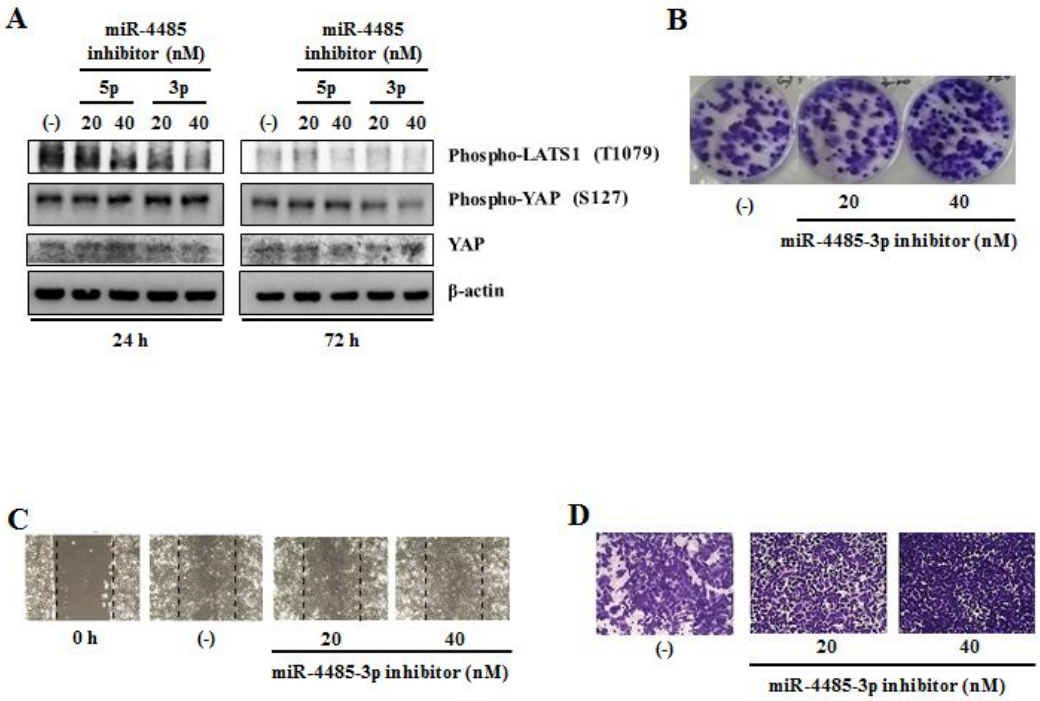
A
miR-4485 inhibitor (nM)
5p
3p
(-) 20 40 20 40
(-) 20 40 20 40
Phospho-LATS1 (T1079)
Phospho-YAP (S127)
YAP
β-actin
24 h
72 h
B
(-)
20
40
miR-4485-3p inhibitor (nM)
C
0 h
(-)
20
40
miR-4485-3p inhibitor (nM)
D
(-)
20
40
miR-4485-3p inhibitor (nM)

Figure 11. miR-4485 inhibitor activates the Hippo signaling pathway and induces migration and invasion

(A) Cells were treated with miR-4485 inhibitor for 24 h with indicated concentrations. The lysates were analyzed by western blot analysis with antibody against LATS1 and YAP using β-actin as a loading control. (B) The inhibitor treated cells were subjected to a colony formation assay. Representative pictures for colony growth are shown. Typical cell colonies observed by bright-field microscopy at day 14 of growth. (C) Migration in miR-4485 inhibitor treated cells was evaluated using wound healing assays. (D) A549 cells were either untreated or treated with the inhibitor for 24 h and subjected to Matrigel-based transwell invasion assays. Invasive cells are imaged in a bright-field microscope.

8. Cytotoxic activity of PsA and its analogues

The cytotoxicity of the prepared PsA (1) and its analogues (**13 – 40**) was evaluated against two human cancer cell lines (A549 lung cancer cell line and HCT116 colon cancer cell line). As shown in Table 2 and 3, variable cytotoxicity was observed depending on the functional group on the phenyl group. The removal of 3-bromide and 4-hydroxy group from 1 decreased cytotoxicity (entry 2, **13**). The hydrophobic tert-butyl group (entry 4, **15**) showed comparable cytotoxicity with PsA itself. In the case of halides, 4-Cl (17) exhibited the highest activity, with the order as follows; 4-Cl > 4-F > 4-Br (entries 5 – 7). An even higher cytotoxicity was observed in the 3,4-dichloride analogue (**19**) compared to 4-Cl (**17**). However, 3,5-dichloride (**20**) and 2,3,5-trichloride (**21**) analogues did not show increased activity. The electron donating alkoxy group showed dramatic activity de-pending on the O-alkyl group. Among the aliphatic alkoxy derivatives (**22 – 26**), 4-ethoxyphenyl analogue (**23**) showed the highest cytotoxicity in the following order; Et > Me ~ cyclopentyl > n-Pr > n-Bu (entries 11 – 14). In the aromatic alkoxy group, 4-benzyloxy analogue (**28**) had comparable cytotoxicity with PsA. However, a loss of activity was observed in the phenyloxy group (**27**). Among the prepared ana-logues, β-naphthyl analogue caused the highest cyto-toxicity (entry 19, **30**). It is notable that the α-naphthyl derivative (**31**) showed complete loss of cytotoxicity. The role of oxime and disulfide in cytotoxicity was ex-amined. The partial or complete loss of cytotoxicity of O-methylated oximes (**33 – 35**) revealed that the free oxime moiety is very important for cytotoxic activity. Additionally, the

importance of disulfide was confirmed by the partial or completely loss of activity in thioether analogue (**36**) and diamidohexane analogue (**37**). Monomeric sulfide and electrophilic terminal chlorides also showed partial or complete loss of activity. These cumulative results suggest that the hydrophobic group in the phenyl group preserved the cytotoxicity, and that the free oxime and disulfide linker is very important for the cytotoxicity against cancer cells.

Based on the SAR study of PsA and its analogues in regard to cytotoxic activity against human cancer cells, compound **30** (entry 19 in Table 2), which showed the highest cytotoxicity among PsA analogues was selected for further detailed mechanism of action studies in A549 human lung cancer cells. Compound **30** exhibited a concentration-dependent growth inhibition against A549 cells with an IC_{50} value of 1.2 μM after a 72 h incubation (Figure 12A). Morphological features with treatment of **30** (0.2 – 1.6 μM) were also very different with a shrunken and sharp shape at the highest concentration (1.6 μM) (Figure 12B).

Table 2. Cytotoxic Activity of PsA and Its Analogues (1)[a]

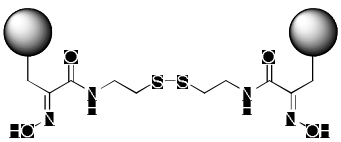

entry	Comp. No	A549[b] $IC_{50}(\mu M)$	HCT116[c] $IC_{50}(\mu M)$
1	3-Br-4-OH-Ph (**1**)	1.18	1.62
2	Ph (**13**)	6.55	6.22
3	4-Me-Ph (**14**)	6.09	5.63
4	4-t-Bu-Ph (**15**)	**1.78**	**1.67**
5	4-F-Ph (**16**)	3.50	3.78
6	4-Cl-Ph (**17**)	2.58	2.03
7	4-Br-Ph (**18**)	5.89	7.24
8	3,4-Cl_2-Ph (**19**)	**1.60**	**1.46**
9	3,5-Cl_2-Ph (**20**)	2.28	2.10
10	2,3,5-Cl_3-Ph (**21**)	5.09	4.23
11	4-MeO-Ph (**22**)	2.81	4.39
12	4-EtO-Ph (**23**)	**1.37**	**1.61**
13	4-*n*-PrO-Ph (**24**)	13.48	15.54
14	4-*n*-BuO-Ph (**25**)	41.13	23.75
15	4-cyclopenthyl-O-Ph (**26**)	1.40	5.34
16	4-PhO-Ph (**27**)	>100	20.35
17	4-BnO-Ph (**28**)	**1.12**	**1.57**

18	4-Nitro-Ph (**29**)	2.66	1.80
19	β-napthyl (**30**)	**1.20**	**1.30**
20	α-napthyl (**31**)	>100	>100
21	9-antracenyl (**32**)	18.47	28.44

[a] All values are means of at least three experiments.

[b]Human lung cancer cells.

[c] Human colon cancer cells.

Table 3. Cytotoxic Activity of PsA Analogues (2)[a]

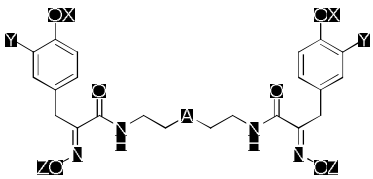

entry	Comp. No	A549[b] IC_{50} (μM)	HCT116[c] IC_{50} (μM)
1	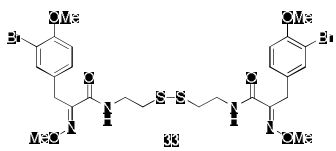	9.2	10.7
2	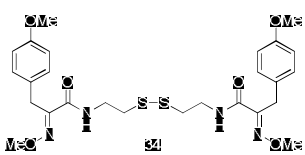	>100	>100
3	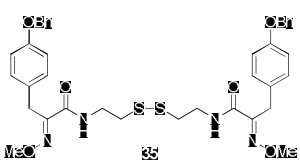	>100	>100
4	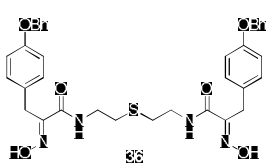	2.5	>100
5	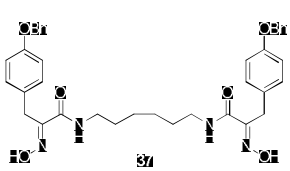	20.1	>100

6	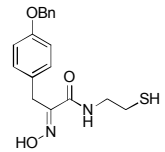 **38**	40.0	85.1
7	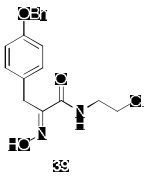 **39**	>100	>100
8	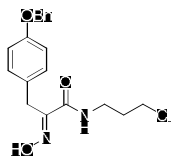 **40**	>100	>100

[a] All values are means of at least three experiments.

[b]Human lung cancer cells.

[c] Human colon cancer cells.

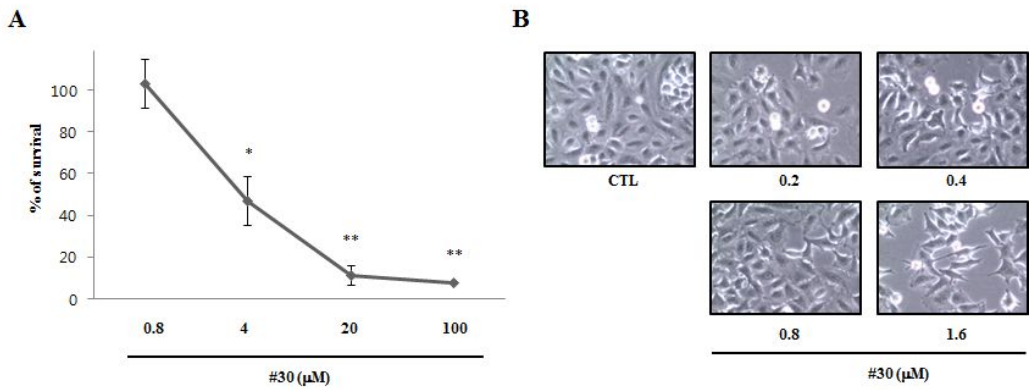

Figure 12. Cytotoxic activity of compound 30

(A) Anti-proliferative activity of compound **30** in cultured human A549 lung cancer cells. (B) Morphological changes were observed. *$p<0.01$; **$p<0.005$, compared with the control.

9. Antitumor effect of compound 30 in a tumor xenograft model

The anti-tumor activity of the test compound was per-formed using an *in vivo* nude mouse xenograft model bearing A549 cells. When the tumor size reached approximately 50 - 60 mm^3 after injection with the A549 cells, compound **30** (15 or 30 mg/kg) or PsA (30 mg/kg) was intraperitoneally administered to mice three times per week. The tumor volume in the control group was approximately 800 mm3 35 days after the cells were subcutaneously implanted into the right flank of each mouse. Paclitaxel (5 mg/kg) was used as a positive control under the same experimental condition. Compared to the vehicle-treated control groups, compound **30** significantly inhibited the tumor growth, and the inhibition rates were 30.4% and 47.6% at 15 mg/kg and 30 mg/kg, respectively, for compound **30** at the end of the experiments (Figure 13A). Tumor weights were also significantly reduced by the treatment with compound **30** (Figure 13C). Similar results were observed in the treatment of PsA. No body weight changes or overt toxicity were observed in the *in vivo* experiment with compound **30** (Figure 13B). Immunohistochemical analysis using the Ki-67 antibody also showed that compound **30** inhibited the expression of the proliferation biomarker Ki-67 in both central and edge region of tumor tissues (Figure 13D). Additionally, hematoxylin and eosin staining data revealed that although there was no significant change in cell number in the central region, the cells in the edge or peripheral region of tumor tissues were significantly reduced, suggesting that the outgrowth of tumor size was inhibited by compound **30** in the *in*

vivo xenograft models (Figure 13D).

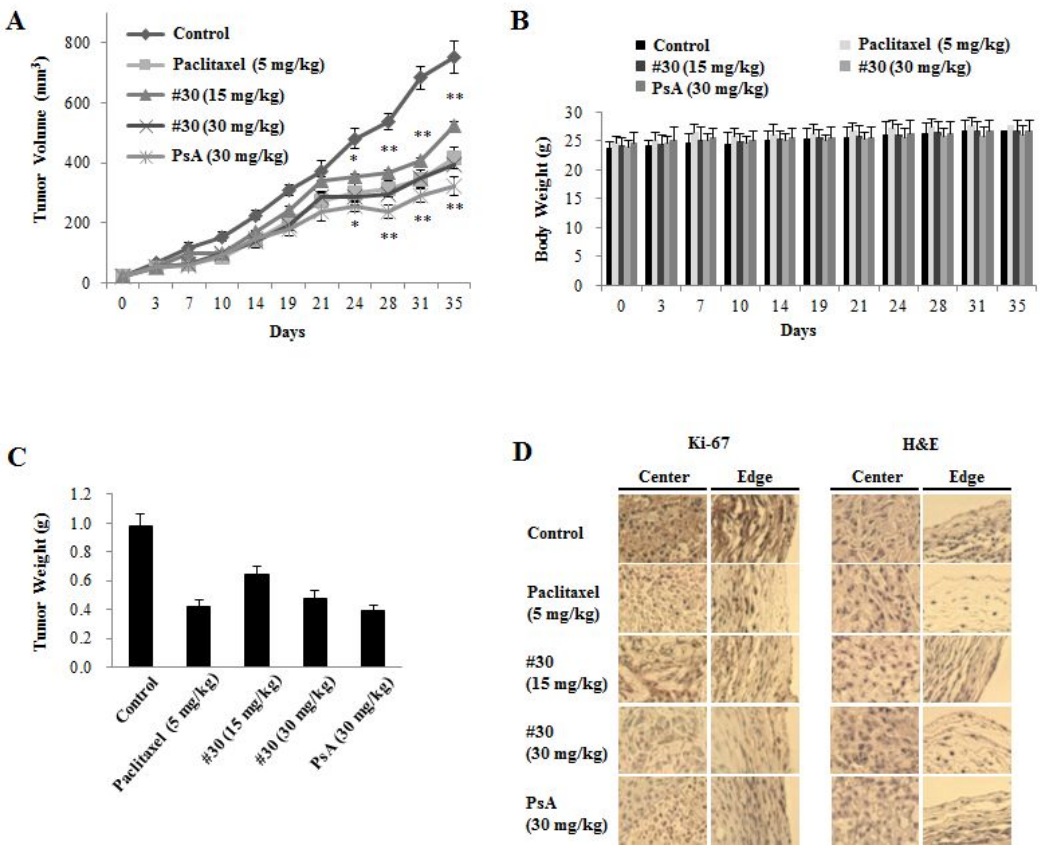

Figure 13. Antitumor effect of compound 30 in a tumor xenograft model

During the experimental procedure, the volume of tumors (A) and the weight of end-point tumor tissues (B) were measured. (C) Tumor weights were also significantly reduced. (D) The tumor sections were also stained by immunohistochemistry method for Ki-67 and H&E.*$p < 0.05$; **$p < 0.01$, compared with the control.

D. Discussion

The results of this study suggest that PsA and miR-4485 have effects on the Hippo pathway in A549 human lung cancer cells. Several studies support this relationship between PsA and the Hippo signaling pathway. First, in A549 cell lines, treatment of PsA or miR-4485 mimic up-regulates the protein level of phospho-YAP, and in turn inactivates of the Hippo signaling pathway. Additionally, these effects of Hippo signaling inactivation can be reversed by forced transfection of miR-4485 inhibitor. Secondly, inactivation of the Hippo signaling pathway reduces colony formation, migration, and invasion of the A549 cells. Thirdly, the results of *in vivo* experiment indicated that PsA inhibits xenograft tumor tissues. These results from both cell-based and *in vivo* experiments suggest that PsA may negatively regulate the Hippo signaling pathway in A549 human lung cancer cells.

Next, based on the potential biological activity of PsA, structure-activity relationship study with synthetic PsA analogues on cancer cells was performed to assess cytotoxicity of the synthetic PsA analogues. Additionally, the functionality of chemical structures were set up to better understand the biological activity of PsA and its analogues. The free oxime group and disulfide functional group were responsible for the high degree of cytotoxicity. However, the bromotyrosine component was relatively tolerable and hydrophobic aromatic groups preserved the cytotoxicity. The cytotoxicity of aromatic group is dependent on the size and spatial geometry. One analogue, β-naphthyl derivative of PsA (compound **30**) was considered as a promising candidate with high cytotoxic activity. Mechanism of

action study of compound **30** also revealed that the compound inhibits HDAC enzymatic activity (data not shown) and *in vivo* tumor growth in murine xenograft models. The *in vivo* antitumor activity of PsA analogue is reported for the first time in this study.

As the Hippo signaling pathway is known to be a regulator of cancer stem cells [39] and is involved in cell adhesion and migration, which are closely associated with cancer progression and metastasis [40]. Targeting the Hippo pathway is a new approach for cancer drug development [41]. In human non-small cell lung cancer (NSCLC), the Hippo signaling pathway and some of its downstream genes, such as CTGF, Gli2 and BIRC5, are associated with the occurrence and development of the disease [42]. Therefore, blocking the Hippo signaling pathway by PsA and its analogues might be a novel therapeutic strategy in cancer treatment.

In Hippo signaling pathway, the mechanism of YAP stability regulation is not clear. YAP is negatively regulated by a core cassette complex consisted of LATS1, LATS2, MST1, and MST2 kinases [43]. In human NSCLC, LATS1 expression has been shown to be associated with YAP expression [44], and MST1 overexpression enhances YAP phosphorylation at Ser127 site [45].

In summary, we report that PsA treatment promotes cytosolic retention of phospho-YAP via up-regulating the protein level of phospho-YAP, and this modulation of YAP may impair migratory and invasive activity of A549 human lung cancer cells. These results provide interesting insights about crosstalk between PsA, derived from marine natural products and the Hippo signaling pathway.

Part III: Antimetastatic Effect of Halichondramide in PC3 Human Prostate Cancer Cells

A. Introduction

Natural products have served as important sources in drug discovery and development [46]. Although most of the current natural product-derived therapeutic drugs originated from terrestrial plant extracts marine-based natural products are recently considered to be an important resource for procurement of new chemical entities [47]. In particular, many compounds derived from marine sponges have exhibited anticancer activities with diverse mechanisms of action [48]. Eribulin mesylate, a structurally simplified macrolactone derivative of halichondrin B, which was originally isolated from the marine sponge *Halichondria okadai*, is an example of recently approved anticancer drug for metastatic breast cancer [49]. Moreover, in a previous study, oxazole-containing macrolides isolated from the marine sponge *Chondrosia corticata* exhibited potential cytotoxicity and antifungal activity [50]. Recently, the antiproliferative effect of (19Z)-halichondramide, a trisoxazole-containing macrolide from *C. corticata*, on human lung cancer cells via G2/M cell cycle arrest and suppression of mTOR signaling pathway was also reported [51]. However, the mechanism underlying the antimetastatic activity of trisoxazole-containing macrolides from *C. corticata* has not yet been elucidated.

Cancer metastasis is considered to be a major cause of cancer death. Indeed, the acquired increase in motility and invasiveness of cancer cells enhance the metastatic processes from the primary sites to secondary tissues [52]. Many distinctive biomarkers are eventually involved in each step of metastasis.

The phosphatase of regenerating liver (PRL) represents a novel subfamily of

protein tyrosine phosphatases (PTPs); this subfamily contains three members (PRL-1, PRL-2, and PRL-3) that share a high degree (75%) of amino acid sequence identity [53]. In particular, PRL-3 has recently attracted a great deal of attention because of its association with tumor metastasis [54]. Elevated PRL-3 mRNA levels have been found in many cancer cells including colon, lung, and prostate. In addition, PRL-3 overexpression was found in nearly all metastatic lesions that are derived from colorectal cancers [55]. Recent findings also suggested that overexpression of PRL-3 promotes motility and metastasis of mouse melanoma cells both *in vitro* cell culture and *in vivo* mouse model [56]. These data might provide PRL-3 as a novel biomarker in association with the metastatic properties of tumor cells. However, little is known about the underlying mechanisms by which PRL-3 promotes cell invasion and growth. In this study, I report for the first time that halichondramide (HCA), a trisoxazole-containing macrolide isolated from *C. corticata*, exhibits potent antimetastatic activity in human prostate cancer cells with the modulation of both PRL-3 and various metastasis biomarkers.

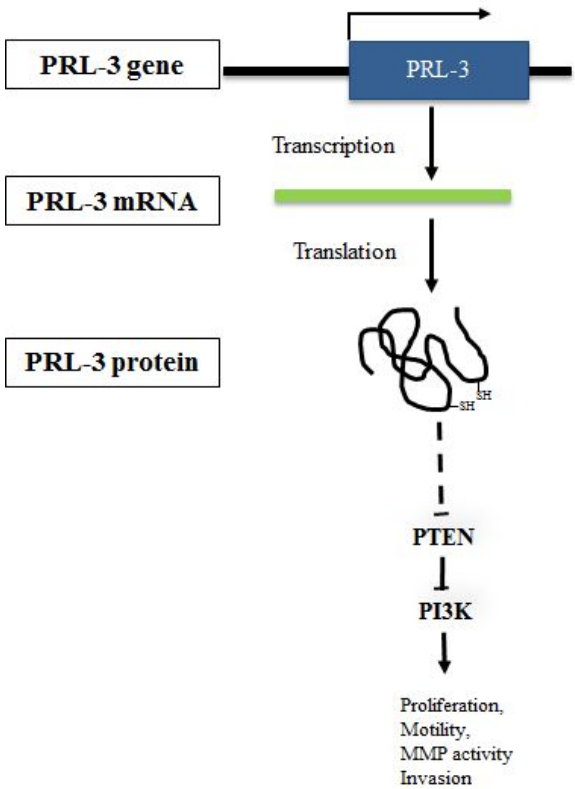

Figure 14. The schematic diagram of PRL-3 and down-stream signaling pathway

B. Materials and Methods

1. Materials

1. 1. Reagents and antibodies

Dimethyl sulfoxide (DMSO), bicinchoninic acid (BCA), copper sulfate, trichloroacetic acid (TCA), and thiazolyl blue tetrazolium bromide (MTT) were purchased from Sigma-Aldrich (St. Louis, MO, USA). Roswell Park Memorial Institute (RPMI) 1640 medium, fetal bovine serum (FBS), trypsin-EDTA solution (1×), and antibiotic-antimycotic solution (100×) were purchased from Invitrogen (Carlsbad, CA, USA). Mouse monoclonal anti-E-cadherin and anti-N-cadherin were purchased from BD Biosciences (San Diego, CA, USA). Rabbit polyclonal anti-p85, anti-p110, anti-MMP2, and anti-MMP9 were purchased from Cell Signaling Biotechnology (Danvers, MA, USA). Mouse monoclonal anti-PRL-3 was purchased from Santa Cruz Biotechnology (Santa Cruz, CA, USA). The test compound halichondramide (HCA), a trisoxazole-containing macrolide (Figure 6), was isolated from the marine sponge *Chondrosia corticata* in accordance with previously described methods [50] and dissolved in 100% dimethyl sulfoxide (DMSO).

1. 2. Compounds

The test compound halichondramide (HCA), a trisoxazole-containing macrolide (Figure 15), was isolated from the marine sponge *Chondrosia corticata* in

accordance with previously described methods [50] and dissolved in 100% dimethyl sulfoxide (DMSO).

1. 3. Cell culture

The Human prostate adenocarcinoma PC3 cells were obtained from the American Type Culture Collection (Manassas, VA, USA), and were cultured in RPMI-1640 medium supplemented with 10% heat-inactivated fetal bovine serum, 100 units/mL penicillin, 100 μg/mL streptomycin, and 250 ng/mL amphotericin B at 37 °C in a humidified incubator under an atmosphere containing 5% CO_2.

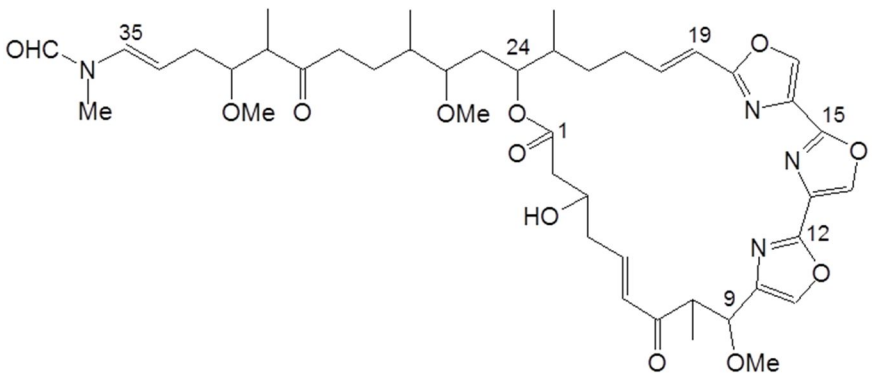

Figure 15. Chemical structure of halichondramide

2. Methods

2. 1. The Evaluation of Antiproliferation Activity

Cell proliferation was measured using the sulforhodamine B (SRB) assay [57]. Briefly, PC3 cells (4×10^4 cells/mL) were seeded in 96-well plates with various concentrations of HCA and incubated at 37 °C in a humidified atmosphere with 5% CO2. After 72 h of HCA treatment, the cells were fixed with a 10% TCA solution for 1 h, and cellular proteins were stained with 0.4% SRB in a 1% acetic acid solution. The stained cells were dissolved in 10 mM Tris buffer (pH 10.0). The effect of HCA on cell proliferation was calculated as a percentage, relative to a solvent-treated control, and the IC_{50} values were determined using nonlinear regression analysis (percent survival versus concentration).

2. 2. Analysis of Gene Expression by Real-Time RT-PCR

The Real-time RT-PCR was employed to determine the gene expression of PRL-3 in PC3 cells. Briefly, PC3 cells (2×10^5 cells/mL) were cultured in 100 mm dishes for 24 h. The cells were treated with HCA for an additional 24 h. Total cellular RNA was extracted with TRIzol reagent and reverse transcribed at 42 °C for 60 min with 0.5 μg of oligo(dT)15 primer in a reaction volume of 20 μL, using reverse transcription system (Promega, MI, USA). Specific gene primers were designed and were subsequently custom synthesized by Bioneer Corporation (Daejon, Korea). The primer sequences that were used in this study are listed in Table 1. Real-time PCR was conducted using a MiniOpticon system (Bio-Rad,

Hercules, CA, USA); each PCR amplification included 5 μL of reverse transcription product, iQ SYBR Green Supermix (Bio-Rad, Hercules, CA, USA), and primers in a total volume of 20 μL. The following standard thermo cycler conditions were employed: 95 °C for 20 s prior to the first cycle; 40 cycles of 95 °C for 20 s, 56 °C for 20 s, and 72 °C for 30 s; 95 °C for 1 min; and 55 °C for 1 min. The threshold cycle (CT), indicating the fractional cycle number at which the amount of amplified target gene reaches a fixed threshold for each well, was determined using the MJ Opticon Monitor software package (Bio-Rad, Hercules, CA, USA). Relative quantification, representing the change in gene expression in real-time quantitative PCR experiments between a sample-treated group and the untreated control group, was calculated by the comparative CT method in accordance with previously described methods [58]. The data were analyzed by evaluating the expression $2^{-\Delta\Delta CT}$, where $\Delta\Delta CT$ = (CT of target gene − CT of housekeeping gene)treated group – (CT of target gene − CT of housekeeping gene)untreated control group. For the treated samples, the evaluation of $2^{-\Delta\Delta CT}$ represents the fold change in gene expression relative to the untreated control, normalized to a housekeeping gene (β-actin). Real-time PCR primer sequences are listed in Table 4.

Table 4. The sequences of the primer pairs that were used to examine specific target genes in RT-PCR analysis.

Target gene		Sequences
PRL-3	Sense	5′-AGA AGT ACG GGG CTA CCA CTG-3′
	Antisense	5′-CAC AAC GGT GAT GCC ATC CTT-3′
p85	Sense	5′-CTG CCT CCT AAA CCA CCA AAA-3′
	Antisense	5′-TTC ATA CCG TTG TTG GCT ACA G-3′
p110	Sense	5′-CCA CGA CCA TCA TCA GGT GAA-3′
	Antisense	5′-CCT CAC GGA GGC ATT CTA AAG T-3′
E-cadherin	Sense	5′-CGA GAG CTA CAC GTT CAC GG-3′
	Antisense	5′-GGG TGT CGA GGG AAA AAT AGG-3′
N-cadherin	Sense	5′-AGC CAA CCT TAA CTG AGG AGT-3′
	Antisense	5′-GGC AAG TTG ATT GGA GGG ATG-3′
β-Actin	Sense	5′-AGC ACA ATG AAG ATC AAG AT-3′
	Antisense	5′-TGT AAC GCA ACT AAG TCA TA-3′
MMP2	Sense	5′-GAT ACC CCT TTG ACG GTA AGG A-3′
	Antisense	5′-CCT TCT CCC AAG GTC CAT AGC-3′
MMP9	Sense	5′-TGT ACC GCT ATG GTT ACA CTC G-3′
	Antisense	5′-GGC AGG GAC AGT TGC TTC T-3′

2. 3. Western Blot Analysis

Cells were treated with the test compound with various concentrations for 24 h. Each sample was homogenized in ice-cold 1× ProPrep buffer (iNtRON Biotechnology, Seoul, Korea) and incubated for 20 min on ice. The lysates were centrifuged at 12,000× g for 20 min, and the supernatant was collected and stored at −80 °C. Total protein contents were determined using the BCA method. Proteins (30 μg) were denatured by boiling in a lysis buffer (250 mM Tris-HCl at pH 6.8, 4% SDS, 10% glycerol, 0.006% bromophenol blue, 2% β-mercaptoethanol and 2 mM sodium ortho-vanadate) for 5 min. The same amount of protein in each lysate was

loaded and separated by SDS–polyacrylamide gel electrophoresis and then electrotransferred to a PVDF membrane. Nonspecific binding was blocked with 5% BSA in TBS; subsequently, the membranes were incubated with primary antibodies diluted in TBS-Tween 20 containing 3% BSA (1:200–1:1000) overnight at 4 °C, washed three times with TBS-Tween 20, and incubated with corresponding HRP-conjugated secondary antibodies. The protein was detected using a LAS-1000 Imager (Fuji Film Corp., Tokyo, Japan).

2. 4. Wound Healing Assay

To assess the motility of cells exposed to the test compound, a wound healing assay was performed [59]. PC3 cells were seeded in six-well plates at a density of 1×10^5 cells/mL and incubated for 48 h until they reached 80%–90% confluency. A confluent monolayer of PC3 cells was artificially wounded with a micropipette tip, and the detached cells were washed with serum-free RPMI1640 and treated with test compounds in growing medium for 72 h. The cells were washed twice with phosphate-buffered saline. Images of the wounds were photographed at 0 and 72 h under an inverted microscope (CKX41, Olympus).

2. 5. Cell Migration Assay

PC3 cells (1×10^5 cells/chamber) were used for migration assays as described previously [60]. Cells were seeded into the top chambers of a 24-well Matrigel-coated polyethylene terephthalate membrane inserts with 8 μm pores (Millipore, Billerica, MA, USA). The plates were coated with 10 μL of type I collagen (0.5 mg/mL) and

20 μL of a 1:2 mixture of Matrigel:RPMI1640. Cells were plated in the upper chamber of the Matrigel-coated Transwell insert. The medium of the lower chambers also contained 0.1 mg/mL bovine serum albumin as a chemoattractant. The inserts were incubated for 24 h at 37 °C. The cells that had invaded the outer surface of the membrane were fixed with methanol, stained with hematoxylin and eosin, and photographed.

2. 6. Gelatin Zymography

HT-1080 cells were treated with various concentrations of HCA. After 72 h of incubation, conditioned media were collected, and gelatin zymographic analysis was performed to measure the expressions of MMP2 and MMP9 [61]. Briefly, the protein lysates extracted from the conditioned media were denatured by mixing 5× gel loading buffer containing 0.1 M Tris (pH 6.8), 50% glycerol, 2% SDS, and 0.1% bromophenol and electrophoretically separated on a polyacrylamide gel containing 0.2% gelatin. The resolved proteins in the gel were washed and renatured by the exchange of SDS with nonionic detergent Triton X-100 contained in washing buffer (50 mM Tris–HCl, pH 7.5, 100 mM NaCl and 2.5% Triton X-100), and further incubated with incubation buffer (50 mM Tris-HCl at pH 7.5, 150 mM NaCl, 10 mM $CaCl_2$, 0.02% NaN_3, and 1 μM $ZnCl_2$) for 24 h at 37 °C with shaking. The incubated gel was stained with Coomassie Blue R-250, and the proteolytic activities of the MMPs were detected against a blue background as clear bands that resulted from the degradation of gelatin.

2. 7. Statistical analysis

The data are expressed as means ± S.D. The statistical analysis of the data was performed using SigmaStat 2.03 (SPSS, Chicago, IL, USA). One-way analysis of variance (ANOVA) was used to compare the mean responses among the treatments. A statistical probability of $P < 0.05$ was considered significant.

C. Results

1. Growth inhibitory activity of halichondramide in PC3 prostate cancer cells

Antiproliferative potential of halichondramide (HCA) in PC3 human prostate cancer cells was evaluated using the sulforhodamine B (SRB) assay. As illustrated in Figure 16A, HCA exhibited antiproliferative activity against PC3 cells in a concentration-dependent manner, and the IC_{50} value was 0.81 μM for an incubation of 72 h. In particular, the highest concentration (2.5 μM) of HCA produced a remarkable decrease in cell numbers (Figure 16B), suggesting that HCA might exhibit a cytostatic effect at relatively low concentrations but exert a cytotoxic effect at higher concentrations.

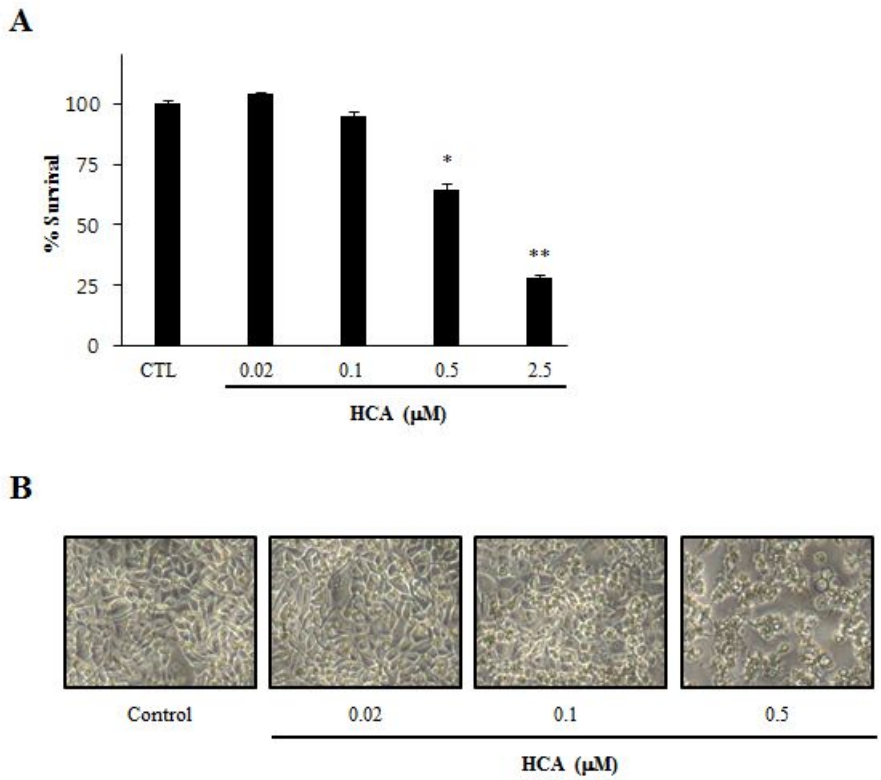

Figure 16. The growth inhibitory activity of HCA in PC3 prostate cancer cells

(**A**) PC3 cells (1×10^5 cells/mL) were treated with HCA for 72 h; subsequently, antiproliferative activity was determined by the SRB protein dye method as described in the Experimental Section. The data are represented as the mean percentages ± SD for each HCA-treated group relative to the DMSO-treated control group. Each experiment was performed in triplicate ($n = 3$). * $p < 0.05$, ** $p < 0.01$ compared with the control group. (**B**) The morphological changes of PC3 cells treated with HCA for 72 h were observed under a phase-contrast microscope and photographed (at 40× magnification).

2. Modulation of the gene expression levels of PRL-3, MMPs, and cadherins by HCA

The modulation of epithelial-mesenchymal transition (EMT) is regarded as an important target in metastatic regulation. To evaluate whether HCA is able to suppress the metastatic potential of highly metastatic cancer cells, the modulation of the expression of genes associated with metastasis, was examined using real-time RT-PCR analysis. HCA significantly down-regulated the mRNA expressions of matrix metalloproteinase-2 (MMP2), MMP9, and N-cadherin, whereas the expression of E-cadherin was upregulated after treatment with HCA for 24 h (Figure 17). In addition, HCA suppressed the expression of PRL-3, a metastasis-associated marker, and of the PI3 kinase subunits p85 and p110, which are downstream targets of PRL-3. These results suggest that HCA is a potential inhibitor of EMT in human adenocarcinoma prostate cancer cells via modulation of PRL-3 and its downstream targets including PI3 kinase.

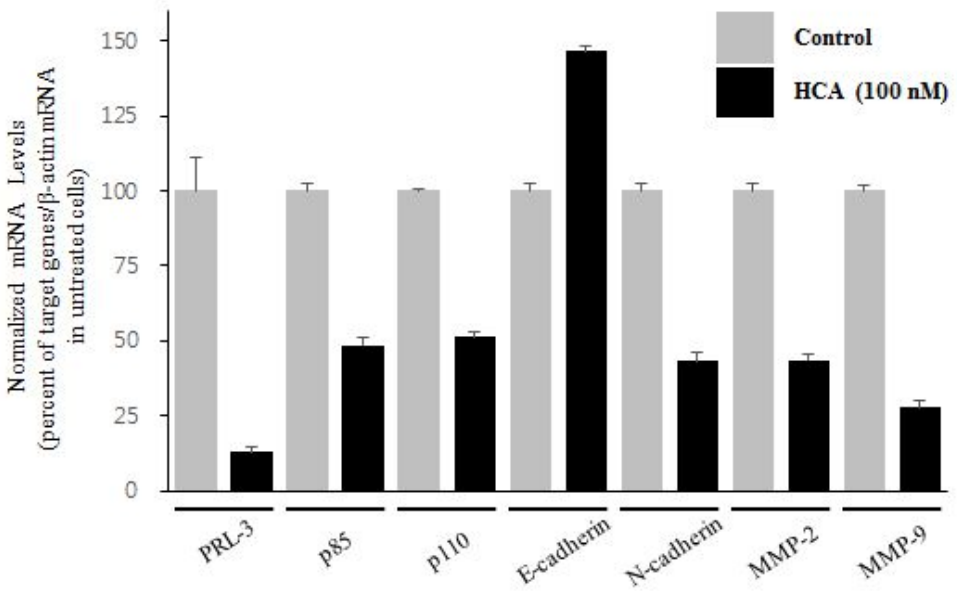

Figure 17. The effects of HCA on the mRNA expression of PRL-3 and its down-stream genes and metastatic biomarkers

PC-3 cells (4×10^5 cells/mL) were treated with HCA for 24 h, and the mRNA expression levels of PRL-3 and metastasis biomarkers were determined by real-time RT-PCR analysis. The data represent the mean values ± SD of nine experiments. * $p < 0.05$, ** $p < 0.01$ compared with the control group.

3. Suppression of expression of PRL-3 and its associated proteins by HCA

To further clarify the mechanisms of action underlying the antimetastatic activity of HCA, signaling proteins that are overexpressed or inactivated in PC3 cells were examined by western blot analysis. These analyses revealed that HCA treatment resulted in the down-regulation of the PRL-3 protein, which is known to be overexpressed in many metastatic cancer cell lines [55a, 62]; these findings are consistent with the suppression of the mRNA expression of PRL-3 by HCA. The pivotal downstream effector proteins of PRL-3, p85 and p110 were also suppressed by HCA (Figure 18). The effect of HCA on metastasis-associated protein expression levels were further examined and it was found that the expression levels of MMP2 and MMP9 were significantly suppressed by HCA. In addition, evaluation of E-cadherin and N-cadherin, additional cancer metastasis biomarkers known to act as a switch in epithelial-mesenchymal transition[63], revealed upregulation of E-cadherin but downregulation of N-cadherin following HCA treatment, further supporting the antimetastatic effects of HCA (Figure 18). These data suggest that the antimetastatic activity of HCA is associated with the modulation of PRL-3, PI3 kinase, and EMT-related proteins in PC3 cells.

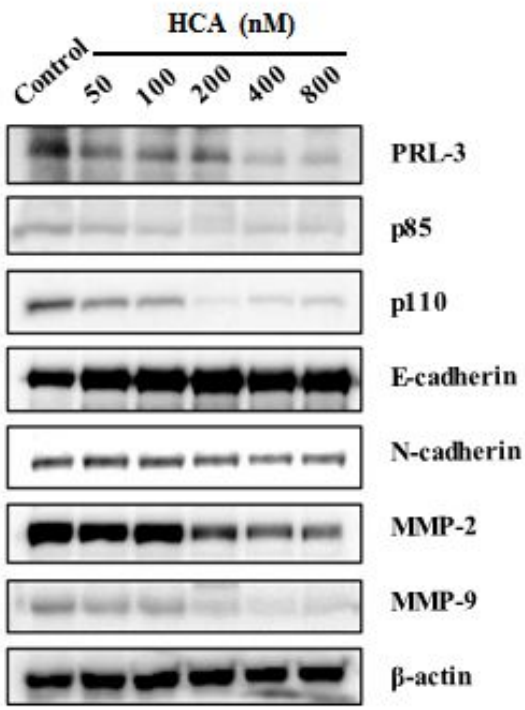

Figure 18. The effects of HCA on the expression of PRL-3 and its associated proteins

PC-3 cells (2×10^5 cells/mL) were treated with HCA for 24 h; subsequently, the protein expression levels of PRL-3 and its associated proteins were analyzed by Western blotting as described in the Experimental Section.

4. Inhibitory effect of HCA on cell migration and invasion

Cellular migration and invasiveness are fundamental features of cancer metastasis. Given the suppressive effects of HCA on expression of genes associated with metastasis, as depicted in Figure 18, further investigations were initiated to confirm the antimetastatic potential of HCA with respect to cellular migration and invasion. Wound healing and invasion assays were performed to evaluate the inhibitory effect of HCA on the migratory features of PC3 cells. In the wound healing assay, a wound scratch in vehicle-treated control cells was almost completely closed after 72 h of incubation. However, treatment with HCA resulted in the suppression of wound healing in a concentration-dependent manner (Figure 19A). In the invasion assay, HCA also demonstrated concentration-dependent inhibition of the invasion of PC3 cells through the embedded inner chamber (Figure 19B).

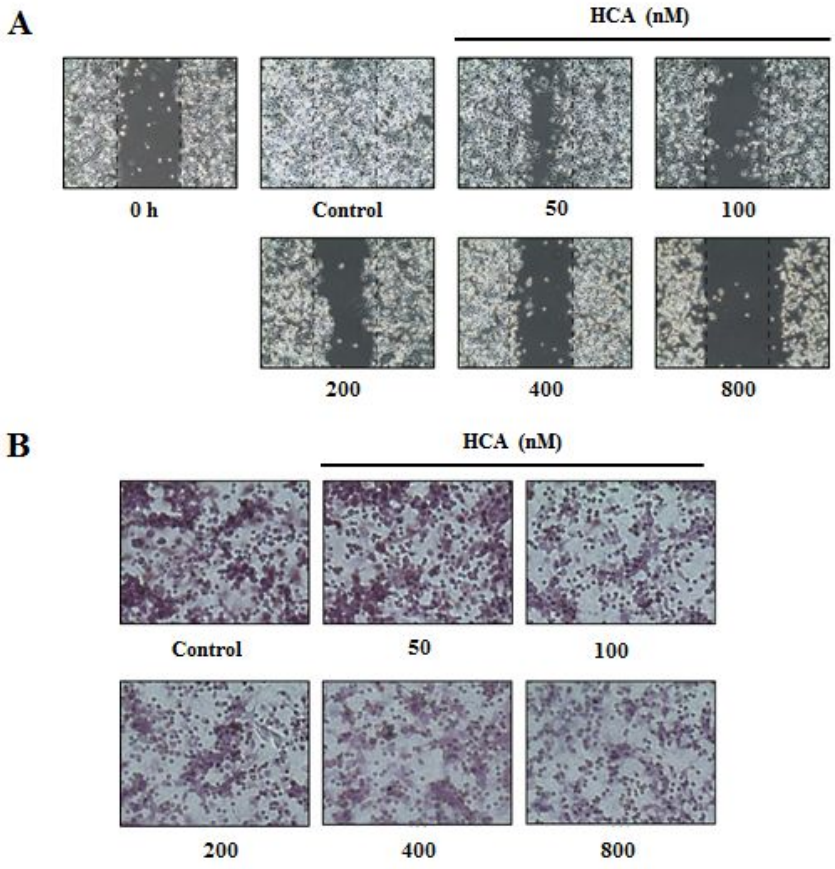
A
HCA (nM)
0 h
Control
50
100
200
400
800
B
HCA (nM)
Control
50
100
200
400
800

Figure 19. The inhibitory effects of HCA on cell migration and invasion

(**A**) The effect of HCA on cell migration was analyzed by the wound healing assay. PC3 cells (1×10^5 cells/mL) were seeded in six-well plates and incubated for 48 h. An artificial wound was made that consisted of a scratch with a micropipette tip. The wound healing process was monitored during 72 h of incubation with various concentrations of HCA. Images of the wounds were photographed at 0 and 72 h under an inverted microscop; (**B**) The cell invasion assay was performed in a Matrigel-coated chamber system as described in the Experimental Section. PC3 cells (1×10^5 cells/chamber) were plated in the upper chambers of Matrigel-coated Transwell insert. The lower chamber contained 0.1 mg/mL BSA as a chemoattractant in the medium. The inserts were incubated for 24 h; subsequently, the cells that had invaded the outer surface of the membrane were fixed, stained, and photographed.

5. Suppressive effect of HCA on MMPs in gelatin zymography

To further determine whether HCA might affect the expression of MMP2 and MMP9, gelatin zymographic analysis was performed in HT-1080 human fibrosarcoma cells. The cells (5×10^4 cells/mL) were treated with HCA for 72 h; following this treatment, protein lysates were resolved on a 0.2% gelatin-containing SDS-polyacrylamide gel. The degradation of the gelatin substrate by the MMP2 and MMP9 was clearly detected in untreated control cells, whereas treatment with HCA markedly inhibited the expressions of MMP2 and MMP9 in a concentration-dependent manner (Figure 20). This result is well correlated with the down-regulation of MMP-2 and MMP-9 protein expression by HCA in PC3 cells (Figure 18).

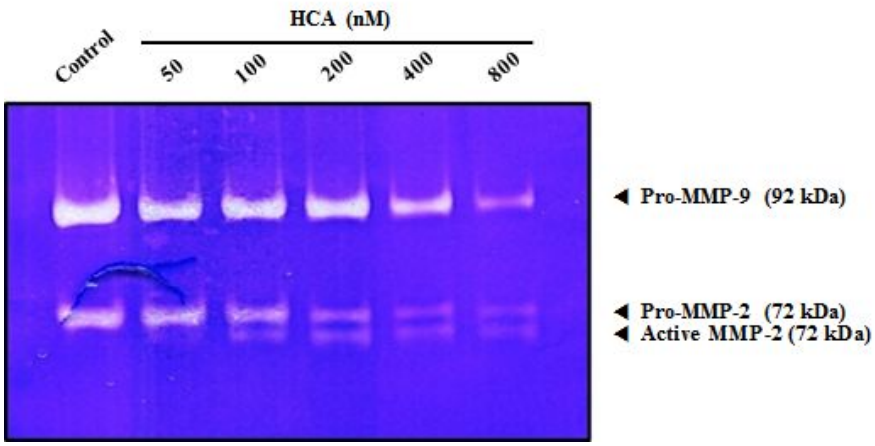

Figure 20. The inhibitory effects of HCA on gelatin degradation

The effect of HCA on the MMPs expression were also analyzed by the gelatin zymographic method. HT-1080 cells (5×10^4 cells/mL) were treated with HCA for 72 h; subsequently, as described in the Experimental Section, the proteolytic activities of the MMPs were assessed by the degradation of gelatin.

D. Discussion

Metastasis of cancer cells is an important factor associated with cancer related deaths [64]. Increase in motility and invasiveness of cancer cells has also been found to be associated with an enhanced tendency to undergo epithelial-mesenchymal transition (EMT) [65]. In particular, functional cadherins are highly associated with the progression of EMT. For example, upregulation of N-cadherin induces invasiveness of tumor cells, whereas loss of E-cadherin also enhances destruction of cell-cell adhesion junctions, and thus these events are considered to be one of the important contributors of EMT [65].

In this study, the antiproliferative and antimetastatic activities of halichondramide (HCA) in human prostate cancer cells were demonstrated. The antiproliferative activities of trisoxazole-containing macrolides, including HCA against a variety of human cancer cell lines, such as lung (A549), colon (HCT116), breast (MDA-MB-231), liver (SK-HEP-1), and stomach (SNU601) cancers, have recently been reported by our group [51]. In agreement with the previous results, HCA exhibited antiproliferative activity against the highly metastatic human PC3 prostate cancer cells. Although oxazole-containing macrolides have exhibited antiproliferative activity against cancer cells [51, 66], the antimetastatic effects of these classes of compounds on cancer cells have not previously been reported. Therefore, the antimetastatic potential of HCA using highly metastatic prostate cancer cells was further determined. HCA modulated the expression of various biomarkers that are associated with metastasis, including PRL-3, p85, p110, E-cadherin, N-

cadherin, MMP2, and MMP9, at both the transcriptional and translational levels. Wound healing and Matrigel invasion assays revealed that HCA also inhibited cellular migration and invasion. Recent studies have demonstrated that phosphatase of regenerating liver-3 (PRL-3) is a potential biomarker of cancer metastasis [67]. PRL-3 was first identified as a protein that plays an essential role in cancer metastasis in a genome-wide transcriptional analysis of colorectal cancer samples [62]. Subsequent studies have found that the overexpression of PRL-3 is highly correlated with increased metastasis in human cancers [55a]. This finding suggests that PRL-3 might be a potential target for human cancer therapy, particularly, with respect to cancer metastasis. In the present study, the overexpression of PRL-3 was detected in PC3 cells, and HCA significantly suppressed expression of PRL-3 at both transcriptional and translational levels in these cells. The expression of subunits p85 and p110 of PI3K, one probable downstream target of PRL-3, was also down-regulated by HCA (Figure 14). These results demonstrate the involvement of PRL-3 in metastasis and the potential of HCA for producing antimetastatic effects in cancer cells. In addition, the analysis of EMT biomarkers is indicative of the metastatic characteristics of cancer cells. An examination of cadherins revealed that N-cadherin was highly overexpressed in PC3 cells but E-cadherin, a counterpart of N-cadherin, was maintained at low levels in these cells. However, treatment with HCA suppressed the expression of N-cadherin but activated the expression of E-cadherin in PC3 cells. These results additionally confirmed the antimetastatic potential of HCA in PC3 cells. The suppression of the matrix metalloproteinases MMP2 and MMP9 and the inhibition of the enzymatic

activities of these metalloproteinases further confirmed the antimetastatic and anti-invasive activities of HCA in highly metastatic cancer cells. PRL-3 has been shown to promote the proliferation of various cell lines [68]. The phosphatidylinositol-3-kinase/protein kinase B (PI3K/AKT) signaling pathway is also an important driver of cell proliferation and survival [69]. These findings indicate that HCA down-regulates the expression of PRL-3 and its downstream target PI3K, abrogating PRL-3-mediated AKT activation. This process might represent one plausible mechanism of action underlying the antimetastatic and antiproliferative activity of HCA in human prostate cancer cells. Although, the antimetastatic activity of HCA with modulation of several biomarkers associated with metastasis was found, the precise mechanism of action of HCA is still unclear. Further detailed studies are needed to explore its anticancer activity on prostate cancer cells. Recent metabolomics studies gave important information for the progression of aggressive prostate cancer phenotype by androgen receptor activation [70]. Therefore, this approach might also be applicable to elucidate the further detailed mechanism of action of HCA on prostate cancer cells.

Part IV: Conclusion

The present study aimed to discover novel activities of two bioactive compounds and finally revealed two possible mechanisms that might be used as novel therapeutic targets to treat human lung and prostate cancer. The findings from each study are summarized as follows (Figure 21).

In Part II, the antitumor activity of PsA in human non-small cell lung cancer cell line A549 was identified. Further analysis revealed that PsA downregulated the protein expression of integrin-linked kinase (ILK), a hub molecule in PI3K/AKT signaling pathway, and upregulated phospho-LATS1 and phospho-YAP, which play key roles in Hippo signaling pathway activation. Moreover, colony formation, migration and invasion characteristics of A549 cells were also decreased. The expression of miR-4485, a small non-coding RNA, was significantly increased in PsA-treated A549 cells. Again, the mimic and inhibitor of miR-4485 also modulate the Hippo signaling pathway and the characteristics of A549 cells

Next, twenty eight analogues of PsA were prepared employing the new synthetic approach. Structure-activity relationship study (SAR) for cytotoxicity revealed that the free oxime group and disulfide functional group were responsible for high degree of cytotoxicity. In addition, the bromotyrosine component was relatively tolerable and hydrophobic aromatic groups preserved the cytotoxicity. The cytotoxicity of aromatic group is dependent on the size and spatial geometry. Among them, compounds **30** showed comparable cytotoxicity to PsA and exhibited potential *in vivo* antitumor activity.

In Part III, The antimetastatic activity of HCA in the highly metastatic PC3 human prostate cancer cells was identified. HCA showed potent growth inhibitory

activity on the PC3 cells with potent IC_{50} value. Further analysis revealed that HCA suppressed the expression of potential metastatic biomarkers, including phosphatase of regenerating liver-3 (PRL-3), phosphoinositide 3-kinase (PI3K) subunits, cause downregulation of matrix metalloproteases (MMPs), and also modulates cadherin switches in PC3 cells. HCA also demonstrated concentration-dependent inhibition of the both migration and invasion of PC3 cells.

The present studies are important as they explored the novel mechanisms of actions of two bioactive natural products, which were proven to be potential therapeutic agents for human lung and prostate cancer.

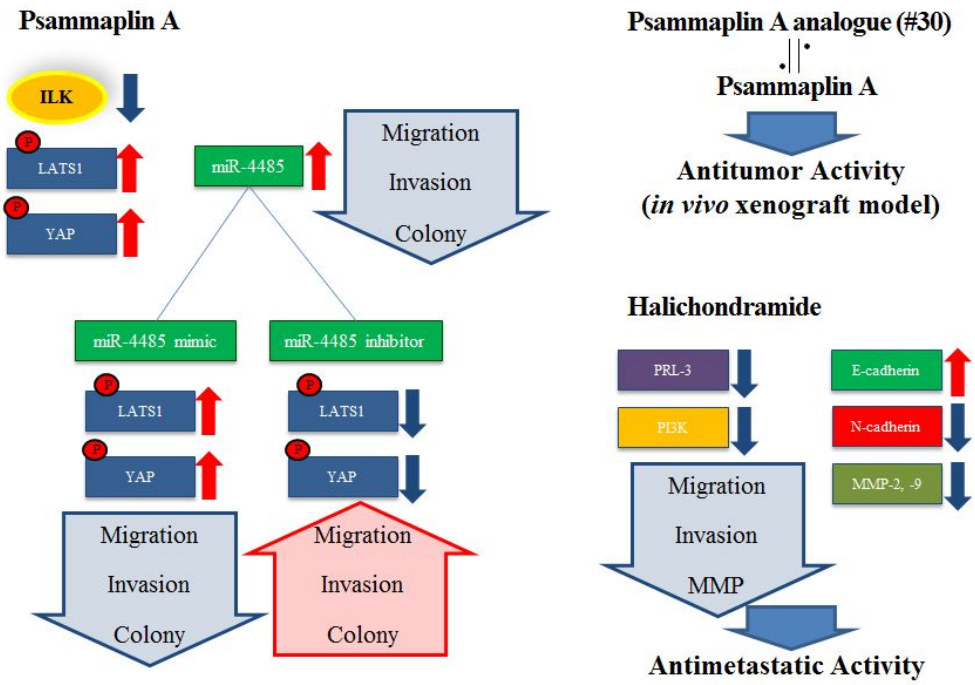

Figure 21. Overview of the mechanism of PsA and HCA

References

1. Esposito, L.; Conti, D.; Ailavajhala, R.; Khalil, N.; Giordano, A., Lung Cancer: Are we up to the Challenge? *Current genomics* **2010,** *11* (7), 513-8.

2. Riihimaki, M.; Hemminki, A.; Fallah, M.; Thomsen, H.; Sundquist, K.; Sundquist, J.; Hemminki, K., Metastatic sites and survival in lung cancer. *Lung cancer* **2014,** *86* (1), 78-84.

3. O'Mahony, D.; Kummar, S.; Gutierrez, M. E., Non-small-cell lung cancer vaccine therapy: a concise review. *Journal of clinical oncology : official journal of the American Society of Clinical Oncology* **2005,** *23* (35), 9022-8.

4. Harvey, K. F.; Pfleger, C. M.; Hariharan, I. K., The Drosophila Mst ortholog, hippo, restricts growth and cell proliferation and promotes apoptosis. *Cell* **2003,** *114* (4), 457-67.

5. (a) Harvey, K.; Tapon, N., The Salvador-Warts-Hippo pathway - an emerging tumour-suppressor network. *Nature reviews. Cancer* **2007,** *7* (3), 182-91; (b) Grusche, F. A.; Richardson, H. E.; Harvey, K. F., Upstream regulation of the hippo size control pathway. *Current biology : CB* **2010,** *20* (13), R574-82.

6. Zeng, Q.; Hong, W., The emerging role of the hippo pathway in cell contact inhibition, organ size control, and cancer development in mammals. *Cancer cell* **2008,** *13* (3), 188-92.

7. (a) Edgar, B. A., From cell structure to transcription: Hippo forges a new path. *Cell* **2006,** *124* (2), 267-73; (b) Zhao, B.; Li, L.; Lei, Q.; Guan, K. L., The Hippo-YAP pathway in organ size control and tumorigenesis: an updated version. *Genes & development* **2010,** *24* (9), 862-74.

8. (a) Xu, Z. P.; Zhu, J. S.; Zhang, Q.; Wang, X. Y., A breakdown of the Hippo pathway in gastric cancer. *Hepato-gastroenterology* **2011,** *58* (110-111), 1611-7; (b) Song, M.; Cheong, J. H.; Kim, H.; Noh, S. H.; Kim, H., Nuclear expression of Yes-associated protein 1 correlates with poor prognosis in intestinal type gastric cancer. *Anticancer research* **2012,** *32* (9), 3827-34.

9. (a) Chen, D.; Sun, Y.; Wei, Y.; Zhang, P.; Rezaeian, A. H.; Teruya-Feldstein, J.; Gupta, S.; Liang, H.; Lin, H. K.; Hung, M. C.; Ma, L., LIFR is a breast cancer metastasis suppressor upstream of the Hippo-YAP pathway and a prognostic marker. *Nature medicine* **2012,** *18* (10), 1511-7; (b) Yu, F. X.; Zhao, B.; Panupinthu, N.; Jewell, J. L.; Lian, I.; Wang, L. H.; Zhao, J.; Yuan, H.; Tumaneng, K.; Li, H.; Fu, X. D.; Mills, G. B.; Guan, K. L., Regulation of the Hippo-YAP pathway by G-protein-coupled receptor signaling. *Cell* **2012,** *150* (4), 780-91.

10. (a) Zhao, B.; Li, L.; Wang, L.; Wang, C. Y.; Yu, J.; Guan, K. L., Cell detachment activates the Hippo pathway via cytoskeleton reorganization to induce anoikis. *Genes & development* **2012,** *26* (1), 54-68; (b) Halder, G.; Dupont, S.; Piccolo, S., Transduction of mechanical and cytoskeletal cues by YAP and TAZ. *Nature reviews. Molecular cell biology* **2012,** *13* (9), 591-600.

11. (a) Serrano, I.; McDonald, P. C.; Lock, F. E.; Dedhar, S., Role of the integrin-linked kinase (ILK)/Rictor complex in TGFbeta-1-induced epithelial-mesenchymal transition (EMT). *Oncogene* **2013,** *32* (1), 50-60; (b) McDonald, P. C.; Fielding, A. B.; Dedhar, S., Integrin-linked kinase--essential roles in physiology and cancer biology. *Journal of cell science* **2008,** *121* (Pt 19), 3121-32.

12. Hannigan, G.; Troussard, A. A.; Dedhar, S., Integrin-linked kinase: a cancer therapeutic target unique among its ILK. *Nature reviews. Cancer* **2005,** *5* (1), 51-63.

13. Serrano, I.; McDonald, P. C.; Lock, F.; Muller, W. J.; Dedhar, S., Inactivation of the Hippo tumour suppressor pathway by integrin-linked kinase. *Nature communications* **2013,** *4*, 2976.

14. (a) Lee, R. C.; Feinbaum, R. L.; Ambros, V., The C. elegans heterochronic

gene lin-4 encodes small RNAs with antisense complementarity to lin-14. *Cell* **1993,** *75* (5), 843-54; (b) Lagos-Quintana, M.; Rauhut, R.; Lendeckel, W.; Tuschl, T., Identification of novel genes coding for small expressed RNAs. *Science* **2001,** *294* (5543), 853-8.

15. Kozomara, A.; Griffiths-Jones, S., miRBase: integrating microRNA annotation and deep-sequencing data. *Nucleic acids research* **2011,** *39* (Database issue), D152-7.

16. Medina, P. P.; Slack, F. J., microRNAs and cancer: an overview. *Cell cycle* **2008,** *7* (16), 2485-92.

17. Carthew, R. W.; Sontheimer, E. J., Origins and Mechanisms of miRNAs and siRNAs. *Cell* **2009,** *136* (4), 642-55.

18. Sethupathy, P.; Megraw, M.; Hatzigeorgiou, A. G., A guide through present computational approaches for the identification of mammalian microRNA targets. *Nature methods* **2006,** *3* (11), 881-6.

19. (a) Alexiou, P.; Vergoulis, T.; Gleditzsch, M.; Prekas, G.; Dalamagas, T.; Megraw, M.; Grosse, I.; Sellis, T.; Hatzigeorgiou, A. G., miRGen 2.0: a database of microRNA genomic information and regulation. *Nucleic acids research* **2010,** *38* (Database issue), D137-41; (b) Xiao, F.; Zuo, Z.; Cai, G.; Kang, S.; Gao, X.;

Li, T., miRecords: an integrated resource for microRNA-target interactions. *Nucleic acids research* **2009,** *37* (Database issue), D105-10.

20. Sporn, M. B., The war on cancer. *Lancet* **1996,** *347* (9012), 1377-81.

21. Ksiazkiewicz, M.; Markiewicz, A.; Zaczek, A. J., Epithelial-mesenchymal transition: a hallmark in metastasis formation linking circulating tumor cells and cancer stem cells. *Pathobiology : journal of immunopathology, molecular and cellular biology* **2012,** *79* (4), 195-208.

22. Zeisberg, M.; Neilson, E. G., Biomarkers for epithelial-mesenchymal transitions. *The Journal of clinical investigation* **2009,** *119* (6), 1429-37.

23. Kraljevic Pavelic, S.; Sedic, M.; Bosnjak, H.; Spaventi, S.; Pavelic, K., Metastasis: new perspectives on an old problem. *Molecular cancer* **2011,** *10*, 22.

24. (a) Brabletz, T., To differentiate or not--routes towards metastasis. *Nature reviews. Cancer* **2012,** *12* (6), 425-36; (b) Lee, J. M.; Dedhar, S.; Kalluri, R.; Thompson, E. W., The epithelial-mesenchymal transition: new insights in signaling, development, and disease. *The Journal of cell biology* **2006,** *172* (7), 973-81.

25. Turley, E. A.; Veiseh, M.; Radisky, D. C.; Bissell, M. J., Mechanisms of

disease: epithelial-mesenchymal transition--does cellular plasticity fuel neoplastic progression? *Nature clinical practice. Oncology* **2008,** *5* (5), 280-90.

26. (a) Kim, D. H.; Shin, J.; Kwon, H. J., Psammaplin A is a natural prodrug that inhibits class I histone deacetylase. *Experimental & molecular medicine* **2007,** *39* (1), 47-55; (b) Ahn, M. Y.; Jung, J. H.; Na, Y. J.; Kim, H. S., A natural histone deacetylase inhibitor, Psammaplin A, induces cell cycle arrest and apoptosis in human endometrial cancer cells. *Gynecologic oncology* **2008,** *108* (1), 27-33.

27. Hong, S.; Shin, Y.; Jung, M.; Ha, M. W.; Park, Y.; Lee, Y. J.; Shin, J.; Oh, K. B.; Lee, S. K.; Park, H. G., Efficient synthesis and biological activity of Psammaplin A and its analogues as antitumor agents. *European journal of medicinal chemistry* **2015,** *96*, 218-30.

28. (a) Quinoa, E.; Crews, P., Phenolic Constituents of Psammaplysilla. *Tetrahedron Lett* **1987,** *28* (28), 3229-3232; (b) Arabshahi, L.; Schmitz, F. J., Brominated Tyrosine Metabolites from an Unidentified Sponge. *J Org Chem* **1987,** *52* (16), 3584-3586; (c) Rodriguez, A. D.; Akee, R. K.; Scheuer, P. J., 2 Bromotyrosine Cysteine Derived Metabolites from a Sponge. *Tetrahedron Lett* **1987,** *28* (42), 4989-4992.

29. Kim, D.; Lee, I. S.; Jung, J. H.; Yang, S. I., Psammaplin A, a natural

bromotyrosine derivative from a sponge, possesses the antibacterial activity against methicillin-resistant Staphylococcus aureus and the DNA gyrase-inhibitory activity. *Archives of pharmacal research* **1999,** *22* (1), 25-9.

30. Jung, J. H.; Sim, C. J.; Lee, C. O., Cytotoxic compounds from a two-sponge association. *J Nat Prod* **1995,** *58* (11), 1722-6.

31. Kim, D.; Lee, I. S.; Jung, J. H.; Lee, C. O.; Choi, S. U., Psammaplin A, a natural phenolic compound, has inhibitory effect on human topoisomerase II and is cytotoxic to cancer cells. *Anticancer research* **1999,** *19* (5B), 4085-90.

32. Shin, J.; Lee, H. S.; Seo, Y.; Rho, J. R.; Cho, K. W.; Paul, V. J., New bromotyrosine metabolites from the sponge Aplysinella rhax. *Tetrahedron* **2000,** *56* (46), 9071-9077.

33. Mora, F. D.; Jones, D. K.; Desai, P. V.; Patny, A.; Avery, M. A.; Feller, D. R.; Smillie, T.; Zhou, Y. D.; Nagle, D. G., Bioassay for the identification of natural product-based activators of peroxisome proliferator-activated receptor-gamma (PPARgamma): the marine sponge metabolite psammaplin A activates PPARgamma and induces apoptosis in human breast tumor cells. *J Nat Prod* **2006,** *69* (4), 547-52.

34. Pina, I. C.; Gautschi, J. T.; Wang, G. Y.; Sanders, M. L.; Schmitz, F. J.;

France, D.; Cornell-Kennon, S.; Sambucetti, L. C.; Remiszewski, S. W.; Perez, L. B.; Bair, K. W.; Crews, P., Psammaplins from the sponge Pseudoceratina purpurea: inhibition of both histone deacetylase and DNA methyltransferase. *J Org Chem* **2003,** *68* (10), 3866-73.

35. (a) Khan, O.; La Thangue, N. B., HDAC inhibitors in cancer biology: emerging mechanisms and clinical applications. *Immunology and cell biology* **2012,** *90* (1), 85-94; (b) Beumer, J. H.; Tawbi, H., Role of histone deacetylases and their inhibitors in cancer biology and treatment. *Current clinical pharmacology* **2010,** *5* (3), 196-208.

36. Ellis, L.; Hammers, H.; Pili, R., Targeting tumor angiogenesis with histone deacetylase inhibitors. *Cancer letters* **2009,** *280* (2), 145-53.

37. (a) Prince, H. M.; Bishton, M. J.; Harrison, S. J., Clinical studies of histone deacetylase inhibitors. *Clinical cancer research : an official journal of the American Association for Cancer Research* **2009,** *15* (12), 3958-69; (b) Marks, P. A.; Xu, W. S., Histone deacetylase inhibitors: Potential in cancer therapy. *Journal of cellular biochemistry* **2009,** *107* (4), 600-8.

38. (a) Cincinelli, R.; Musso, L.; Giannini, G.; Zuco, V.; De Cesare, M.; Zunino, F.; Dallavalle, S., Influence of the adamantyl moiety on the activity of biphenylacrylohydroxamic acid-based HDAC inhibitors. *European journal of*

medicinal chemistry **2014,** *79*, 251-9; (b) Hansen, F. K.; Sumanadasa, S. D.; Stenzel, K.; Duffy, S.; Meister, S.; Marek, L.; Schmetter, R.; Kuna, K.; Hamacher, A.; Mordmuller, B.; Kassack, M. U.; Winzeler, E. A.; Avery, V. M.; Andrews, K. T.; Kurz, T., Discovery of HDAC inhibitors with potent activity against multiple malaria parasite life cycle stages. *European journal of medicinal chemistry* **2014,** *82*, 204-13.

39. (a) Lian, I.; Kim, J.; Okazawa, H.; Zhao, J.; Zhao, B.; Yu, J.; Chinnaiyan, A.; Israel, M. A.; Goldstein, L. S.; Abujarour, R.; Ding, S.; Guan, K. L., The role of YAP transcription coactivator in regulating stem cell self-renewal and differentiation. *Genes & development* **2010,** *24* (11), 1106-18; (b) Zhao, B.; Tumaneng, K.; Guan, K. L., The Hippo pathway in organ size control, tissue regeneration and stem cell self-renewal. *Nature cell biology* **2011,** *13* (8), 877-83; (c) Ramos, A.; Camargo, F. D., The Hippo signaling pathway and stem cell biology. *Trends in cell biology* **2012,** *22* (7), 339-46; (d) Hiemer, S. E.; Varelas, X., Stem cell regulation by the Hippo pathway. *Biochimica et biophysica acta* **2013,** *1830* (2), 2323-34.

40. (a) Lai, D.; Yang, X., BMP4 is a novel transcriptional target and mediator of mammary cell migration downstream of the Hippo pathway component TAZ. *Cellular signalling* **2013,** *25* (8), 1720-8; (b) Artemenko, Y.; Batsios, P.; Borleis, J.; Gagnon, Z.; Lee, J.; Rohlfs, M.; Sanseau, D.; Willard, S. S.; Schleicher, M.; Devreotes, P. N., Tumor suppressor Hippo/MST1 kinase mediates chemotaxis by

regulating spreading and adhesion. *Proceedings of the National Academy of Sciences of the United States of America* **2012,** *109* (34), 13632-7; (c) Artemenko, Y.; Devreotes, P. N., Hippo on the move: tumor suppressor regulates adhesion and migration. *Cell cycle* **2013,** *12* (4), 535-6.

41. Johnson, R.; Halder, G., The two faces of Hippo: targeting the Hippo pathway for regenerative medicine and cancer treatment. *Nature reviews. Drug discovery* **2014,** *13* (1), 63-79.

42. (a) Finger, E. C.; Cheng, C. F.; Williams, T. R.; Rankin, E. B.; Bedogni, B.; Tachiki, L.; Spong, S.; Giaccia, A. J.; Powell, M. B., CTGF is a therapeutic target for metastatic melanoma. *Oncogene* **2014,** *33* (9), 1093-100; (b) Chu, C. Y.; Chang, C. C.; Prakash, E.; Kuo, M. L., Connective tissue growth factor (CTGF) and cancer progression. *Journal of biomedical science* **2008,** *15* (6), 675-85; (c) Yamamoto, H.; Ngan, C. Y.; Monden, M., Cancer cells survive with survivin. *Cancer science* **2008,** *99* (9), 1709-14; (d) Pantazi, E.; Gemenetzidis, E.; Trigiante, G.; Warnes, G.; Shan, L.; Mao, X.; Ikram, M.; Teh, M. T.; Lu, Y. J.; Philpott, M. P., GLI2 induces genomic instability in human keratinocytes by inhibiting apoptosis. *Cell death & disease* **2014,** *5*, e1028.

43. (a) Wang, K.; Degerny, C.; Xu, M.; Yang, X. J., YAP, TAZ, and Yorkie: a conserved family of signal-responsive transcriptional coregulators in animal development and human disease. *Biochemistry and cell biology = Biochimie et*

biologie cellulaire **2009,** *87* (1), 77-91; (b) Harvey, K. F.; Zhang, X.; Thomas, D. M., The Hippo pathway and human cancer. *Nature reviews. Cancer* **2013,** *13* (4), 246-57; (c) Sawada, A.; Kiyonari, H.; Ukita, K.; Nishioka, N.; Imuta, Y.; Sasaki, H., Redundant roles of Tead1 and Tead2 in notochord development and the regulation of cell proliferation and survival. *Molecular and cellular biology* **2008,** *28* (10), 3177-89.

44. Lin, X. Y.; Zhang, X. P.; Wu, J. H.; Qiu, X. S.; Wang, E. H., Expression of LATS1 contributes to good prognosis and can negatively regulate YAP oncoprotein in non-small-cell lung cancer. *Tumour biology : the journal of the International Society for Oncodevelopmental Biology and Medicine* **2014,** *35* (7), 6435-43.

45. Xu, C. M.; Liu, W. W.; Liu, C. J.; Wen, C.; Lu, H. F.; Wan, F. S., Mst1 overexpression inhibited the growth of human non-small cell lung cancer in vitro and in vivo. *Cancer gene therapy* **2013,** *20* (8), 453-60.

46. Blunt, J. W.; Copp, B. R.; Keyzers, R. A.; Munro, M. H.; Prinsep, M. R., Marine natural products. *Natural product reports* **2014,** *31* (2), 160-258.

47. Montaser, R.; Luesch, H., Marine natural products: a new wave of drugs? *Future medicinal chemistry* **2011,** *3* (12), 1475-89.

48. (a) Halim, H.; Chunhacha, P.; Suwanborirux, K.; Chanvorachote, P., Anticancer and antimetastatic activities of Renieramycin M, a marine tetrahydroisoquinoline alkaloid, in human non-small cell lung cancer cells. *Anticancer research* **2011,** *31* (1), 193-201; (b) Nguyen, H. T.; Chau, V. M.; Tran, T. H.; Phan, V. K.; Hoang, T. H.; Nguyen, T. D.; Nguyen, X. N.; Tai, B. H.; Hyun, J. H.; Kang, H. K.; Kim, Y. H., C29 sterols with a cyclopropane ring at C-25 and 26 from the Vietnamese marine sponge Ianthella sp. and their anticancer properties. *Bioorg Med Chem Lett* **2009,** *19* (16), 4584-8; (c) Kijjoa, A.; Wattanadilok, R.; Campos, N.; Nascimento, M. S.; Pinto, M.; Herz, W., Anticancer activity evaluation of kuanoniamines A and C isolated from the marine sponge Oceanapia sagittaria, collected from the Gulf of Thailand. *Marine drugs* **2007,** *5* (2), 6-22.

49. Jain, S.; Vahdat, L. T., Eribulin mesylate. *Clinical cancer research : an official journal of the American Association for Cancer Research* **2011,** *17* (21), 6615-22.

50. Shin, J.; Lee, H. S.; Kim, J. Y.; Shin, H. J.; Ahn, J. W.; Paul, V. J., New macrolides from the sponge Chondrosia corticata. *J Nat Prod* **2004,** *67* (11), 1889-92.

51. Bae, S. Y.; Kim, G. D.; Jeon, J. E.; Shin, J.; Lee, S. K., Anti-proliferative effect of (19Z)-halichondramide, a novel marine macrolide isolated from the

sponge Chondrosia corticata, is associated with G2/M cell cycle arrest and suppression of mTOR signaling in human lung cancer cells. *Toxicology in vitro : an international journal published in association with BIBRA* **2013,** *27* (2), 694-9.

52. Yoon, S. O.; Park, S. J.; Yun, C. H.; Chung, A. S., Roles of matrix metalloproteinases in tumor metastasis and angiogenesis. *Journal of biochemistry and molecular biology* **2003,** *36* (1), 128-37.

53. (a) Diamond, R. H.; Cressman, D. E.; Laz, T. M.; Abrams, C. S.; Taub, R., PRL-1, a unique nuclear protein tyrosine phosphatase, affects cell growth. *Molecular and cellular biology* **1994,** *14* (6), 3752-62; (b) Cates, C. A.; Michael, R. L.; Stayrook, K. R.; Harvey, K. A.; Burke, Y. D.; Randall, S. K.; Crowell, P. L.; Crowell, D. N., Prenylation of oncogenic human PTP(CAAX) protein tyrosine phosphatases. *Cancer letters* **1996,** *110* (1-2), 49-55; (c) Zeng, Q.; Hong, W.; Tan, Y. H., Mouse PRL-2 and PRL-3, two potentially prenylated protein tyrosine phosphatases homologous to PRL-1. *Biochemical and biophysical research communications* **1998,** *244* (2), 421-7.

54. (a) Stephens, B. J.; Han, H.; Gokhale, V.; Von Hoff, D. D., PRL phosphatases as potential molecular targets in cancer. *Mol Cancer Ther* **2005,** *4* (11), 1653-61; (b) Sager, J. A.; Benvenuti, S.; Bardelli, A., PRL-3: a phosphatase for metastasis? *Cancer biology & therapy* **2004,** *3* (10), 952-3.

55. (a) Bardelli, A.; Saha, S.; Sager, J. A.; Romans, K. E.; Xin, B.; Markowitz, S. D.; Lengauer, C.; Velculescu, V. E.; Kinzler, K. W.; Vogelstein, B., PRL-3 expression in metastatic cancers. *Clinical cancer research : an official journal of the American Association for Cancer Research* **2003,** *9* (15), 5607-15; (b) Wang, L.; Shen, Y.; Song, R.; Sun, Y.; Xu, J.; Xu, Q., An anticancer effect of curcumin mediated by down-regulating phosphatase of regenerating liver-3 expression on highly metastatic melanoma cells. *Molecular pharmacology* **2009,** *76* (6), 1238-45.

56. (a) Wu, X.; Zeng, H.; Zhang, X.; Zhao, Y.; Sha, H.; Ge, X.; Zhang, M.; Gao, X.; Xu, Q., Phosphatase of regenerating liver-3 promotes motility and metastasis of mouse melanoma cells. *Am J Pathol* **2004,** *164* (6), 2039-54; (b) Zeng, Q.; Dong, J. M.; Guo, K.; Li, J.; Tan, H. X.; Koh, V.; Pallen, C. J.; Manser, E.; Hong, W., PRL-3 and PRL-1 promote cell migration, invasion, and metastasis. *Cancer Res* **2003,** *63* (11), 2716-22.

57. Jo, S. K.; Hong, J. Y.; Park, H. J.; Lee, S. K., Anticancer Activity of Novel Daphnane Diterpenoids from Daphne genkwa through Cell-Cycle Arrest and Suppression of Akt/STAT/Src Signalings in Human Lung Cancer Cells. *Biomolecules & therapeutics* **2012,** *20* (6), 513-9.

58. Livak, K. J.; Schmittgen, T. D., Analysis of relative gene expression data

using real-time quantitative PCR and the 2(-Delta Delta C(T)) Method. *Methods* **2001,** *25* (4), 402-8.

59. Kim, G. D.; Cheong, O. J.; Bae, S. Y.; Shin, J.; Lee, S. K., 6"-Debromohamacanthin A, a bis (indole) alkaloid, inhibits angiogenesis by targeting the VEGFR2-mediated PI3K/AKT/mTOR signaling pathways. *Marine drugs* **2013,** *11* (4), 1087-103.

60. Hwang, H. J.; Park, H. J.; Chung, H. J.; Min, H. Y.; Park, E. J.; Hong, J. Y.; Lee, S. K., Inhibitory effects of caffeic acid phenethyl ester on cancer cell metastasis mediated by the down-regulation of matrix metalloproteinase expression in human HT1080 fibrosarcoma cells. *The Journal of nutritional biochemistry* **2006,** *17* (5), 356-62.

61. Park, E. J.; Park, H. J.; Chung, H. J.; Shin, Y.; Min, H. Y.; Hong, J. Y.; Kang, Y. J.; Ahn, Y. H.; Pyee, J. H.; Lee, S. K., Antimetastatic activity of pinosylvin, a natural stilbenoid, is associated with the suppression of matrix metalloproteinases. *The Journal of nutritional biochemistry* **2012,** *23* (8), 946-52.

62. Saha, S.; Bardelli, A.; Buckhaults, P.; Velculescu, V. E.; Rago, C.; St Croix, B.; Romans, K. E.; Choti, M. A.; Lengauer, C.; Kinzler, K. W.; Vogelstein, B., A phosphatase associated with metastasis of colorectal cancer. *Science* **2001,** *294* (5545), 1343-6.

63. Araki, K.; Shimura, T.; Suzuki, H.; Tsutsumi, S.; Wada, W.; Yajima, T.; Kobayahi, T.; Kubo, N.; Kuwano, H., E/N-cadherin switch mediates cancer progression via TGF-beta-induced epithelial-to-mesenchymal transition in extrahepatic cholangiocarcinoma. *British journal of cancer* **2011,** *105* (12), 1885-93.

64. Hanahan, D.; Weinberg, R. A., The hallmarks of cancer. *Cell* **2000,** *100* (1), 57-70.

65. Thiery, J. P.; Sleeman, J. P., Complex networks orchestrate epithelial-mesenchymal transitions. *Nature reviews. Molecular cell biology* **2006,** *7* (2), 131-42.

66. Kiyoto, S.; Kawai, Y.; Kawakita, T.; Kino, E.; Okuhara, M.; Uchida, I.; Tanaka, H.; Hashimoto, M.; Terano, H.; Kohsaka, M.; Aoki, H.; Imanaka, H., A New Antitumor Complex, Wf-1360, Wf-1360a, Wf-1360b, Wf-1360c, Wf-1360d, Wf-1360e and Wf-1360f. *J Antibiot* **1986,** *39* (6), 762-772.

67. McParland, V.; Varsano, G.; Li, X.; Thornton, J.; Baby, J.; Aravind, A.; Meyer, C.; Pavic, K.; Rios, P.; Kohn, M., The metastasis-promoting phosphatase PRL-3 shows activity toward phosphoinositides. *Biochemistry* **2011,** *50* (35), 7579-90.

68. (a) Matter, W. F.; Estridge, T.; Zhang, C.; Belagaje, R.; Stancato, L.; Dixon, J.; Johnson, B.; Bloem, L.; Pickard, T.; Donaghue, M.; Acton, S.; Jeyaseelan, R.; Kadambi, V.; Vlahos, C. J., Role of PRL-3, a human muscle-specific tyrosine phosphatase, in angiotensin-II signaling. *Biochemical and biophysical research communications* **2001,** *283* (5), 1061-8; (b) Werner, S. R.; Lee, P. A.; DeCamp, M. W.; Crowell, D. N.; Randall, S. K.; Crowell, P. L., Enhanced cell cycle progression and down regulation of p21(Cip1/Waf1) by PRL tyrosine phosphatases. *Cancer letters* **2003,** *202* (2), 201-11; (c) Ming, J.; Liu, N.; Gu, Y.; Qiu, X.; Wang, E. H., PRL-3 facilitates angiogenesis and metastasis by increasing ERK phosphorylation and up-regulating the levels and activities of Rho-A/C in lung cancer. *Pathology* **2009,** *41* (2), 118-26.

69. Cully, M.; You, H.; Levine, A. J.; Mak, T. W., Beyond PTEN mutations: the PI3K pathway as an integrator of multiple inputs during tumorigenesis. *Nature reviews. Cancer* **2006,** *6* (3), 184-92.

70. (a) Tripathi, P.; Kamarajan, P.; Somashekar, B. S.; MacKinnon, N.; Chinnaiyan, A. M.; Kapila, Y. L.; Rajendiran, T. M.; Ramamoorthy, A., Delineating metabolic signatures of head and neck squamous cell carcinoma: phospholipase A2, a potential therapeutic target. *The international journal of biochemistry & cell biology* **2012,** *44* (11), 1852-61; (b) MacKinnon, N.; Khan, A. P.; Chinnaiyan, A. M.; Rajendiran, T. M.; Ramamoorthy, A., Androgen

receptor activation results in metabolite signatures of an aggressive prostate cancer phenotype: an NMR-based metabonomics study. *Metabolomics* **2012,** *8* (6), 1026-1036.

국문초록

해양 천연물 유래 사마필린 A와 할리콘드라마이드의 항암활성 연구

서울대학교 대학원
약학과
천연물과학 전공
신윤호

다양한 동식물로부터 분리된 천연물은 생리활성을 가지는 물질의 중요한 자원으로 활용되어 왔으며, 인간의 질병을 치료하기 위한 목적으로 다양하게 개발되고 이들의 활성도 많은 연구가 진행되고 있다. 본 연구에서는 해양 천연물에서 유래된 생리활성 천연물인 사마필린A와 할리콘드라마이드가 갖고 있는 우수한 암세포 증식 억제 효능 및 암전이 억제에 대한 연구를 진행하였다.

수행된 연구에서는 아직 명확한 작용기전이 밝혀지지 않은 사마필린A의 작용기전을 밝히고자 하였다. 암세포의 성장에 영향을 미치는 것으로 알려진 Hippo signaling pathway 상의 LATS와 YAP의 단백질 발현을 효과적으로 조절하는 것을 확인할 수 있었고 *in vitro* 상에서의 colony 형성을 억제하였으며, 세포의 이동성과 침윤성도 감소됨이 관찰되었다. 뿐만 아니라 세포의 사멸을 유도하고 세포분열을 억제하는 것을 알 수 있었다. microRNA array를 통하여 사마필린A를

폐암 세포주인 A549에 처리하였을 때 가장 크게 변화하는 miR-4485를 target으로 선별하였다. 실제로 miR-4485의 mimic을 세포주에 주입한 결과 사마필린A를 처리하였을 때와 마찬가지로 Hippo signaling을 조절하고 유사한 세포 현상들이 관찰되었다. 반면에 miR-4485의 inhibitor를 주입한 세포주에서는 mimic과는 반대되는 결과를 얻을 수 있었다.

또한 합성된 사마필린A의 유도체들을 확보하고 구조-활성 관계 연구를 통해 사마필린A와 대등한 세포독성을 가지는 β-napthyl 구조의 유도체를 후보물질로 선별하였다. 면역력이 결핍된 nude mouse를 이용한 xenograft model에서 기존의 사마필린A와 합성된 유도체의 종양 성장억제 효능을 확인한 결과, 이 유도체를 투여한 실험군에서 종양의 성장억제가 뚜렷하게 관찰되었다.

할리콘드라마이드는 전립선암 세포주에서 뚜렷한 독성을 나타내었고 전이성 암세포에서 발현이 증가되어있다고 알려진 PRL-3의 발현을 효과적으로 억제하였다. PRL-3의 하위 signaling에 위치한 PI3K의 subunit도 감소되었으며, Epithelial-Mesenchymal Transition (EMT) 주요한 바이오마커인 cadherin 스위치도 조절하였다. 또한 세포의 이동성과 침윤성이 물질의 농도 의존적으로 감소 하였으며, Extra cellular matrix(ECM) 조절인자인 MMPs의 활성도 조절하는 특성이 있음을 밝혔다.

이러한 결과들을 바탕으로 본 연구에서는 사마필린과 할리콘드라마이드가 가지는 항암 및 항전이 효능에 대한 메커니즘을 규명 하였으며, 각각 Hippo signaling의 비활성과 PRL-3 발현을

감소시킴으로써 폐암과 전립선암을 치료할 수 있는 새로운 후보물질로 제시하고자 한다.

주요어: 해양 천연물, 사마필린, 할리콘드라마이드, 항암 활성, Hippo signaling, miR-4485, PRL-3, 항전이 활성
학번: 2011-21732